國立臺灣大學工學院機械工程研究所

碩士論文

Department of Mechanical Engineering

College of Engineering

National Taiwan University

Master Thesis

藉 Preisach 模型為基礎之遲滯線性化提升

同步壓電平臺伺服性能

Synchronized piezo-actuated stage control using Preisach model

based on phenomenon linearization

徐廣昊

Xu Guanghao

指導教授：顏家鈺 博士

Advisor: Jia-Yush Yen, Ph.D.

中華民國 106 年 7 月

July 2017

國立臺灣大學碩士學位論文
口試委員會審定書

藉 Preisach 模型為基礎之遲滯線性化
提升多軸壓電平台伺服性能
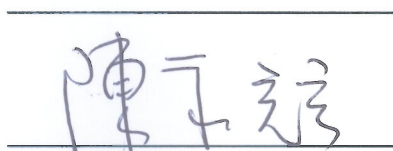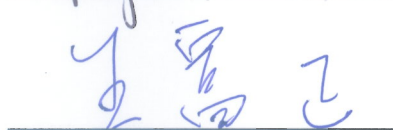## Multi-axes piezo-actuated stage control using Preisach model based hysteresis linearization

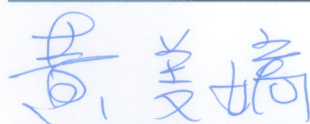本論文係徐廣昊君（R04522839）在國立臺灣大學機械工程學系完成之碩士學位論文，於民國 106 年 7 月 14 日承下列考試委員審查通過及口試及格，特此證明

口試委員：

_____（簽名）

（指導教授）

_____ _____

_____ _____

_____ _____

系主任 _____（簽名）

誌謝

感謝口委老師耐心查看本論文並指正。

`

摘要

壓電制動器具備高位移解析度以及良好之操作頻寬，因此被廣泛應用於微控制系統之中。然而，以壓電材料製成之驅動器在輸入電壓以及位移間含有遲滯所造成之非線性現象，造成控制上的困難，使其定位控制之精確度受到限制。此外，定位之時，雙驅動器位置之不相等亦會阻踞控制成果。

本論文針對遲滯效應所造成的非線性現象做補償，使遲滯對系統所造成的影響線性化，進而提升控制之精確度。依據文獻中提出的電荷控制架構，已知流經壓電制動器之電荷量與其伸長量呈線性關係，因此可藉串接於壓電制動器之電容量測電荷量進而得知遲滯所造成的電壓消耗，以此建立補償器以利補償其非線性效應，並針對已經線性化的系統也設計了位置追蹤補償器。此外，本論文針對硬體架構之特點提出了一種交互耦合控制器以在不同操作頻率之下對雙壓電驅動器所產生的非同步現象進行修正，以簡易且快速之方式大幅提升不同頻率下雙驅動器的同步驅動控制效果。

壓電制動器之模型與分析、參數識別、Preisach 模型之建構、交互耦合控制器的設計方法將在本論文仲介紹與討論。最後佐以不同控制頻率下之驗證結果。

關鍵字：壓電制動器、遲滯補償、Preisach、同步

`

ABSTRACT
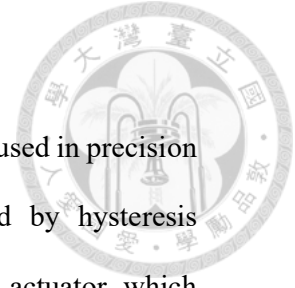
With high resolution and large bandwidth, piezo-actuator is widely used in precision position control system. However, there is nonlinear effect caused by hysteresis phenomenon between input voltage and displacement of the piezo-actuator which increases the difficulty for control, thus degrades the precision of control result. Besides, dual actuators position difference limits the performance as well.

In this thesis, for the sake of enhancing the control performance, the nonlinearity caused by hysteresis phenomenon is compensated, so the system now is a linear mechanic system. Referring to the charge control structure proposed by L.S. Chen et al., it is shown that the relationship between charge flowing through the piezo-actuator and its elongation is linear. Therefore, by measuring the charge flowing through the piezo-actuator, the voltage consumption caused by the hysteresis can be obtained and the hysteresis compensator can be built to compensate the nonlinear effect and then, due to the system can be regarded as a linear mechanic system after being compensated, a tracking controller is designed for positioning. Besides, a cross-coupled controller is designed referring to the hardware structure to fix asynchrony phenomenon under different frequencies on produced by dual-actuators, improves the control results significantly in a simple and rapid pattern.

Piezo-actuator's modeling and analyses, system parameters identification, Preisach model building, cross-coupled controller design method are introduced and discussed in this thesis. For validity, a series of experiments under several frequencies are implemented in this thesis.

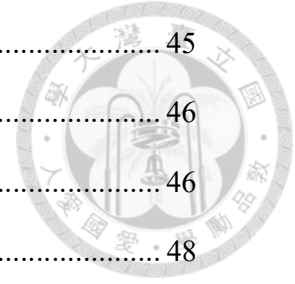Keywords: piezo-actuator, hysteresis compensator, Preisach, synchronization

CONTENTS

`

LIST OF FIGURES

`

LIST OF TABLES

Nomenclature

A	Amplitude of the signal
B	Damping constant of overall system
B_p	Damping constant of piezo actuator
B_s	Damping constant of piezo stage
c_p	Equivalent capacitance of piezo actuator
c_e	External capacitance for measuring charge
f	Frequency
F_{ext}	External force applied on piezo actuator/stage
F_p	Force generated by piezo actuator
$F(\alpha, \beta)$	Preisach function
G	Transfer function of u_p to y
G_{stage}	Transfer function of the stage
G_v	Transfer function of the nominal system
k_1	Equivalent spring constant of the four parallel connected cantilever beams of same axis of the stage
k_3	Spring constant of the cantilever beam suffering from axial compression force.
K	Effective spring constant of the overall system
K_p	Effective spring constant of piezo actuator
K_s	Effective spring constant of piezo stage
M	Mass of the overall system
M_p	Mass of piezo actuator
M_s	Mass of piezo stage
q	Charge flowing through piezo actuator
Q_p	Charge stored in equivalent capacitor

Q_T	Charge stored in electromechanical transducer
R_c	Transfer function of voltage division
T_{em}	Electromechanical transformation ratio
u	Voltage applied to the system
u_{ctrl}	Controlled input voltage applied to the system
u_h	Voltage loss consumed by the hysteretic operator
u_p	Effective voltage applied to the transducer
u_{remain}	Remained voltage after the hysteresis phenomenon
V_e	Voltage on the external capacitance
x	X-direction displacement of the piezo stage
y	Displacement of of the stage
α	Switch on value of hysteron
β	Switch off value of hysteron
γ	Elongation constant
$\hat{\gamma}_{\alpha\beta}$	Backlash operator
$\mu(\alpha,\beta)$	Weighting function of Preisach model
Γ	Effective stiffness between F_p and Δ_p
Δ_p	Elongation of piezo actuator
θ	Rotational displacement of the piezo stage

`

Chapter 1　　Introduction

The first chapter of this thesis will provide a brief overview on how current literature have contributed in the field of hysteresis compensation.

1.1　　Motivation

In nano-position applications, Piezo-actuator is normally used due to high resolution, fast response and large force generation. However, the hysteresis phenomenon of the piezo-actuator, which is regarded as an nonlinear voltage consumption, reduces the effective input voltage and degrades the control performance. Therefore, methodologies in proposing the elimination of the hysteresis phenomenon have been the focus of current literature, from which another alternative proposition will be further discussed in this thesis.

1.2　　Literature Review

To eliminate hysteresis nonlinearity, many methods were proposed. In general, there are two categories of hysteresis compensation: 1) inverse-hysteresis compensation and 2) closed loop hysteresis reduction.

In terms of inverse-hysteresis compensation, the very beginning step is to formulate corresponding inverse model. Then apply this model in a feed-forward compensator.[1][2][3]. The key points of the inverse-hysteresis compensation method is based on the accuracies and precision of the hysteresis model. To obtain a formulated model that as close as possible to real case, complicated calculation is need as a cost. In order to make a balance between model accuracy and calculation efficiency, the polynomial Preisach model[4][5] based on the physical meaning of the hysteresis is proposed. This Preisach model could be formulated as a polynomial equation and is widely used to compensate the hysteresis phenomenon[5]. The model performs well in

1

`

low-frequency but no longer has accurate under high-frequency .when applied under

high-frequency signal, there will be obvious tracking error. To solve this problem,

different approaches such as rate-dependent Presiach models have been discussed for

operations under high speed[7][8][9], nevertheless, those models are not as practical as

the rate-independent ones since they usually require more complicate identification

procedure for formulating the model.

On the other hand, with respect to the closed-loop hysteresis reduction method,

researchers used the feedback controller to eliminate the hysteresis phenomenon[10].

Theoretically, this approach calculates the tracking error which is provided by previous

input signal, so it could not cancel all the hysteresis phenomenon but only constrain it,

but it prevents the complicated hysteresis model identification process.

The hysteresis observer proposed by J. G. Yi *et al.*[11] is a method that estimates the

hysteresis accurately under high frequency operation and is feasible in realization. The

hysteresis, in that theory, is treated as the disturbance[12][13]. The system inversion is

necessary in order to calculate the hysteresis, and the result is used to remove the

hysteresis phenomenon[14]. This method is similar to inverse-hysteresis compensation

but the hysteresis model is not required to be formulated.

The disadvantage of hysteresis observation method is that the grey-box system

identification, which is a complicated procedure, is required. Being the most difficult

method in system ID, the grey-box ID is the most time consuming method, so it is not

adequate for complex systems.

After all, to reduce the complexity of system ID, a modified control structure based

on electromechanical piezo model[15] is proposed by L.S. Chen *et al*[16]. The effective

driving voltage of the piezo-actuator can be obtained by connecting an additional

capacitance to the circuit. The influence of hysteresis can then be decoupled from the

`

system dynamics and the system description could be obtained by a simpler identification method.

The synchronized control of piezo-actuated stage hasn't been researched before, However the methods of other actuated stage may also work in this stage. In general, R.D.Lorenz *et al*[17] and Y.Koren[18] cateloged synchronized control method in three approach: Synchronized master command approach, Master-slave approach and Cross-coupled approach. What's more, adaptive fuzzy control and robust cross-coupled control are used in synchronized control[19][20]. However, those methods are not adopted due to the disadvantages of inaccuracy and demand of control in both low and high frequencies.

1.3   Contributions

The piezo-actuating system used in this thesis is based on the modified structure[16] where the hysteresis phenomenon is served as an additional voltage consumption.

To compensate hysteresis phenomena of different frequencies signals a modified Preisach hysteresis model in this thesis. The hysteresis model is used to linearize the hysteresis by compensating the hysteresis differences. Furthermore, with the same structure, the linearization for hysteresis under different frequencies is achievable.

What's more, a novel method is proposed to provide synchronized control between two axes piezo-actuators. This method is simple but performs well in the condition of not influencing the overall control method.

After conducting a series of experiments, the results show that hysteresis compensator ensures the low and high frequency performance but without the requirement of system in version. Besides, the experimental results with and without synchronized control are shown which indicate this novel synchronized control method

3

`

performs well and could be used in any dual-axis system.

Chapter 2   Hardware Introduction
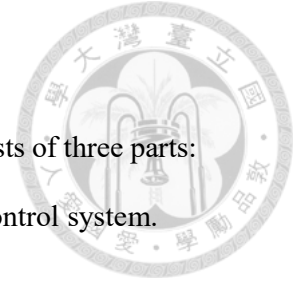
In this chapter. The hardware used in this thesis is introduced, consists of three parts: (1) Piezo-actuated stage (2) Laser measurement system and (3) Servo control system.

2.1   Piezo-actuated Stage

The experimental stage is made of 304 stainless steel on which the proposed control method is validated. Since it is constructed by flexure hinge, both friction and clearance are negligible, the influence of vibration, shock and dirt of the stage are limited. Moreover, lubrication and seal are not necessary, Driven by two pairs of piezos (PSt 150/5x5/7 by Piezomachanilk as shown in Table 2-1), the number of the degrees of freedom is three. The traveling range of x and y axis are $16\mu m$, meanwhile the third freedom θ goes with a pitch/yaw radius of $\pm 100 \, \mu rad$. The movement of this degree is achieved by applying different voltages in two piezos of one pair. To avoid the interference between the stage and other mechanical elements, it is designed to be circular structure with diameter of 90mm and 5mm thickness. The schematic diagram of the piezo-stage is shown in Fig. 2-1.
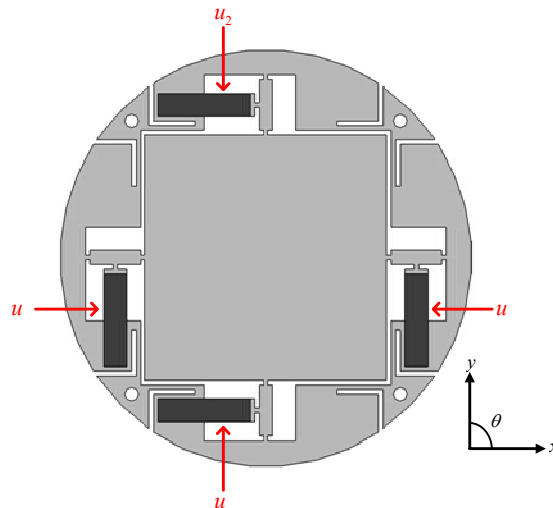
Fig. 2-1 Flexure hinge stage and corresponding input channels

5

`

Ceramic-cross section	$5 \times 5 \text{mm}^2$
Length	18 mm
Maximum stroke	$28/20 \mu\text{m}$
Capacitance	1800nF
Resonance frequency	50kHz
Stiffness	$60\text{N}/\mu\text{m}$
Blocking force	1600N
Maximum load force	2000N

Table 2-1 Detailed specifications of PSt 150/5x5/7 stack piezo actuator [21]

2.2 Displacement Measurement System

Measurement System is very important in this system because it is the information source of the control method. The requirements of the measurement system including high reliability, high resolution and would be better to be non-contact. So the laser interferometer system, which can satisfied those requirements, is chosen for the measurement of the stage displacement. Agilent 10705A, a heterodyne type single beam interferometer with the ability of low frequency noise rejection, is selected as the measurement equipment as the frequency of control reference is relatively low.

2.2.1 Overall Structure of Laser Interferometer System

The overall structure of the laser interferometer system is composed of two paths, as shown in Fig. 2-2 Overall structure of laser interferometer system , called Path A and Path B. The measurement point of Path A is the center of the measured object which mainly indicates the displacement of the system. The measurement point of Path B is on one

6

`

side's edge of measured object from which we can calculate the status of third degree θ.

The reason that we do not put all two path in the front side of measured object is the space

limitation which may cause the measurement instruments interfacing with each other.
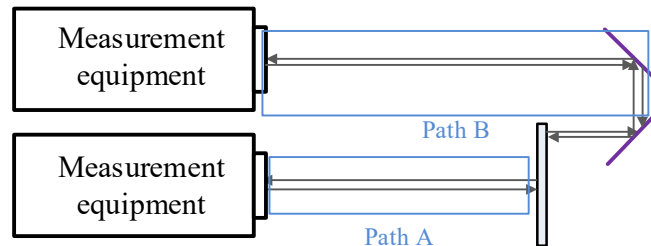
Fig. 2-2 Overall structure of laser interferometer system

2.2.2   One Path Structure of Laser Interferometer System

Take Path A as an example to explain the details of this Laser Interferometer system.

The Path A is composed of four parts: the laser head Agilent 5517C, the path system, the

receiver Agilent 10780C and the axis-board N1231A, as shown in Fig. 2-3. The

specification is listed in Table 2-2.

The measurement procedure starts from laser head, from which the laser beam fires

and the beam goes into path system. Depending on the displacement of measured object,

the path system modifies the laser frequency and changes the beam path to let the laser

beam reflect back to the receiver. A beam splitter, an interferometer and a plane mirror

included in the path system. Through this measurement process, the displacement

information can be converted in to the digital signal using the axis-board with the

Doppler-shift   of   the   received   signal   compared   with   the   original   source.

7

`
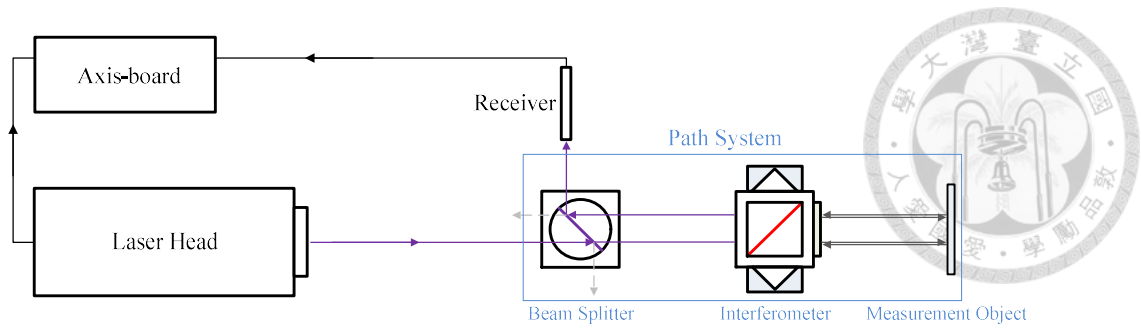
Fig. 2-3 Structure of one path laser interferometer system

Resolution	0.3 nm
Maximum linear velocity	696 mm/s
Reference frequency	2.4 MHz
Output Power	180 μW
1-axis Data collection time	2.5 μs
2-axis Data collection time	3.5 μs
3-axis Data collection time	4.5 μs

Table 2-2 Detailed specifications of laser interferometer system

2.2.3 Laser Path and the Operating Principle of Interferometer

A beam splitter, an interferometer and a plane mirror included in the path system, which is shown in Fig. 2-2.Among all those equipment ,the main element of path system is single beam interferometer. As shown in Fig. 2-4(b),a single beam interferometer contains a quarter wave lens, an one phase reflecting mirror and two rectro-reflectors The rectro-reflector reflects the beam back along the vector that is parallel to the incidence ray. The one-phase reflecting lens reflects the laser with phase equal to 0 or π(cosine phase) in Polar coordinate, but allow the laser with phase equal to 0.5π or 1.5π (sine

8

`

phase)in Polar coordinate to pass through. As for the quarter wave lens, the phase of the laser pass through will be shifted by $1/4_\pi$.

Due to the insufficient space between the laser beam in and reflecting one, the receiver is too big that cannot put in the path system without blocking the incoming laser beam. To solve this problem, a 50% beam splitter (Fig. 2-4 (a)) allocated in front of the interferometer. Although it disperses half the intensity of the laser which is passing through, it changes the direction vertically so that receiver can be alternatively implemented on the side of the beam splitter, and the remaining intensity of the laser is still enough for working.

Fig. 2-4 (a) Beam splitter   (b) The structure of interferometer

Laser beam source Agilent 5517C provides two kinds of lasers with different frequency simultaneously. As shown in Fig, the laser with a higher frequency f_B is a sine wave used for reference laser. On the other hand, a cosine wave with the lower frequency f_A is called measurement laser. Then the two lasers overlap each other and are fired to the interferometer together when they are passing the one-phase reflecting mirror inside the interferometer, they will be divided in to two paths. The two optic paths will be discussed separately.

9
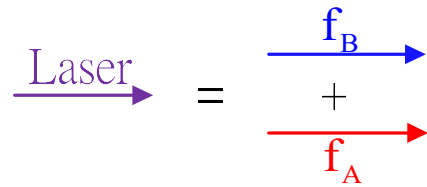
Fig. 2-5 Laser beam consists of two different lasers

On one hand, after reference signal passing through the beam splitter, it fails to go through one-phase reflecting lens in interferometer, installs it is reflected toward rectro-reflector, which reflected back to lens and then back to beam splitter again eventually to receiver . During this process the signal passes beam splitter twice so the power of light in receiver only contains 1/4 part of originally one. The corresponding optic path is shown in Fig. 2-6
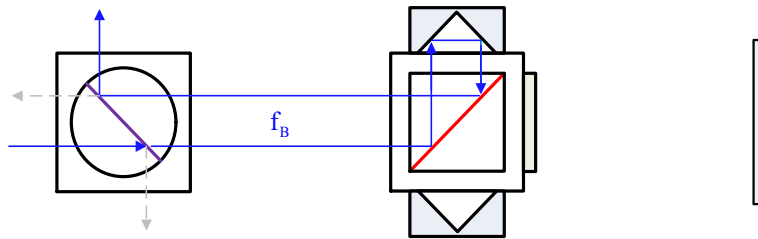
Fig. 2-6 Optic path of the reference laser

One the other hand, the measurement optic path is much more complex. In all there are four states.

Firstly, after dispersed by beam splitter similar to reference signal, the beam can pass though the interferometer and reaches the mirror but with a phase shifted by $1/4\pi$, as shown in Fig. 2-7.
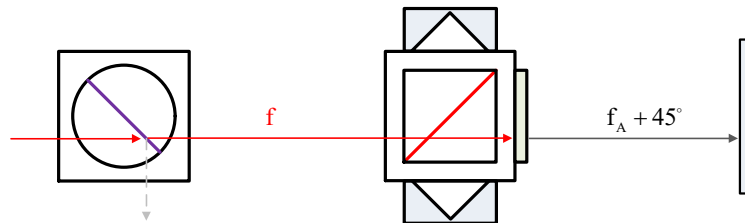
Fig. 2-7 First part of the path of the measurement laser

10

`

Secondly, when the beam passes interferometer then reaches the plane mirror, a Doppler frequency shift of f_Δ caused. And then the beam passes though the quarter-wave lens again with another $1/4_\pi$ radian shift so becomes the cosine wave laser with frequency f_{A2}, which is equal to $f_A + f_\Delta$.
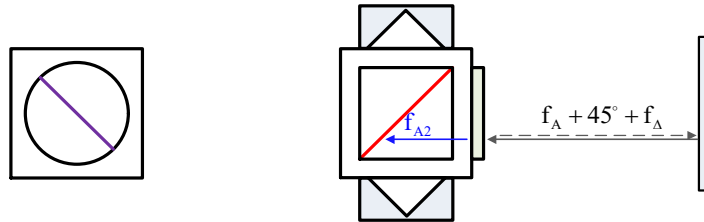
Fig. 2-8 The second part of the measurement path

Thirdly, as reference signal but in the other direction, current signal cannot pass the one-phase reflecting lens as shown in Fig. 2-9, twice reflections in mirror, one more reflection on lens finally direction changes towards plane mirror again.
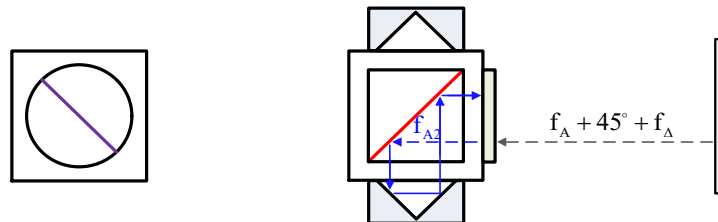
Fig. 2-9 The third part of the measurement path

Fourthly, the same as second state, the laser gets another Doppler frequency shift of f_Δ when reaches plane mirror, so now the frequency f_{A3} is equal to $f_A + 2f_\Delta$, In the end, the beam passes though the interferometer and beam splitter the same as state one and finally reaches receiver. During measurement optic path, the signal goes though beam splitter twice again the same as reference signal. The fourth state is as shown in Fig. 2-10.

11
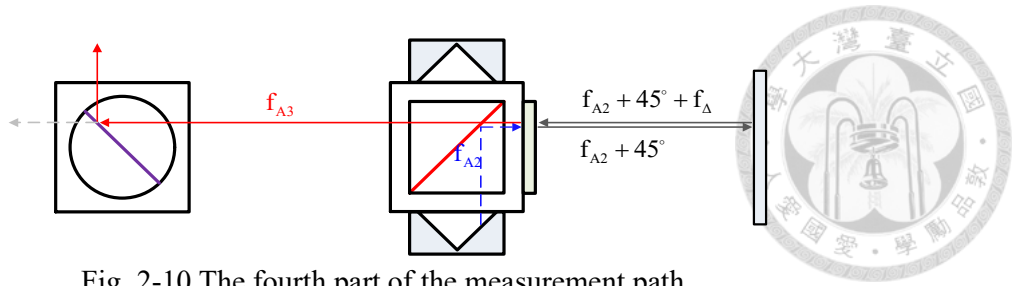
Fig. 2-10 The fourth part of the measurement path

The overall structure of one path of the beam with both the reference and measurement laser is included is as shown in Fig. 2-11.The receiver takes two path's lasers and converts them to digital signal and transmitted to the axis-board. The Doppler frequency shift $2f_\Delta$ caused by plane mirror is used to calculate the plane mirror's displacement. Besides, if the plane mirror is static, the frequency shift $2f_\Delta$ will be equal to zero and resulting measurement value zero as well..
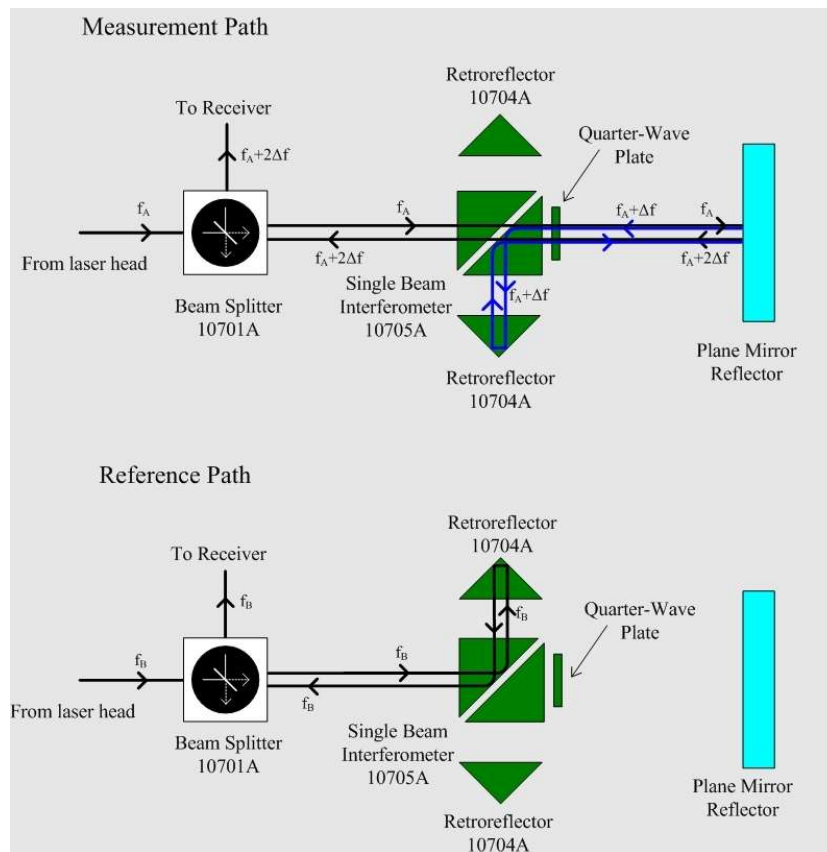
Fig. 2-11 Laser path schematic [33]

12

`

2.3 Hardware and Software of Servo Control System

This section will introduce the hardware architecture and software –hardware integration of Servo Control system, which is the stage applied control method on.

2.3.1 Hardware Architecture

The servo control system includes a PC, a data acquisition (DAQ) board, a laser measurement system (consists of two measurement paths), a charge measurement unit and an amplifier as shown in Fig. 2-12.

The PC uses CPU Intel Core^{TM} 2 DUO E4500 and 2.0 G RAM. The control programs are implemented in the Visual C++ environment and the execution time per loop depends on the sampling rate of the DAQ board. National Instruments PCI-6229 is selected, with four 16-bit analog output channels and thirty-two16-bit analog input channels, it also provides the analog output from -10V to 10V with resolution of $305\mu V$ and has the sampling rate up to 250kHz.The voltage amplifier E-663 (by Physik Instrumente) is an amplifier type specifically designed for the piezo-actuator with the voltage gain of 10±0.1 and the voltage output range from -20 V to 120 V, the response curve of E-633 is shown in Fig. 2-13. The numbers by the curves are the capacitance value of the driven actuator (unit: μF).Final part of the hardware is an external capacitor, chosen as 84uF by connecting eight Mylar capacitors in parallel, as shown in Fig. 2-14.

PC generates the control signal to the DAQ board to produce the analog voltage, and receives measurement data from DAQ board. In order to give the PC enough time to calculate the control signal, the sampling rate of DAQ board is set to be 5 kHz, the operating range of the piezo-actuator is from -10V to 110V, which is far beyond the operating voltage of DAQ board, so an amplifier is chosen. After the amplifier driving the piezo-actuator, the displacement of the stage is measured by the laser interferometer

`

system introduced in Section 2.2. To get more information related with hysteresis compensation which will be discussed in the later chapter, an external capacitor is series-connected to the piezo-actuator so that it can be used by measuring the voltage drop across this capacitor.
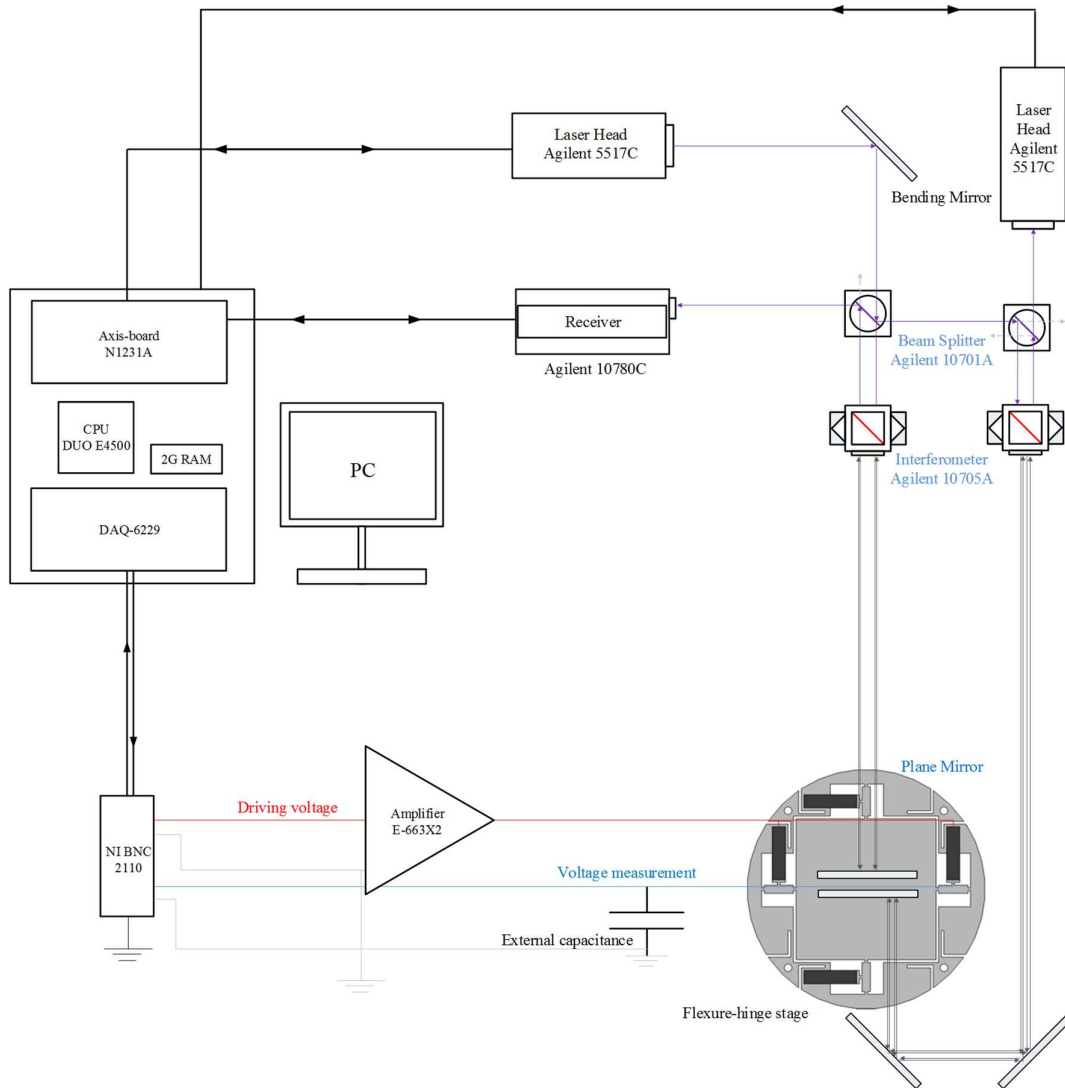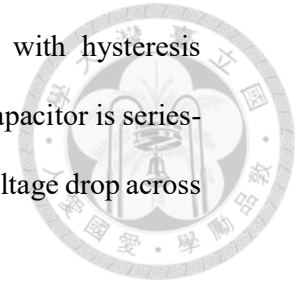
Fig. 2-12 Hardware Architecture

`
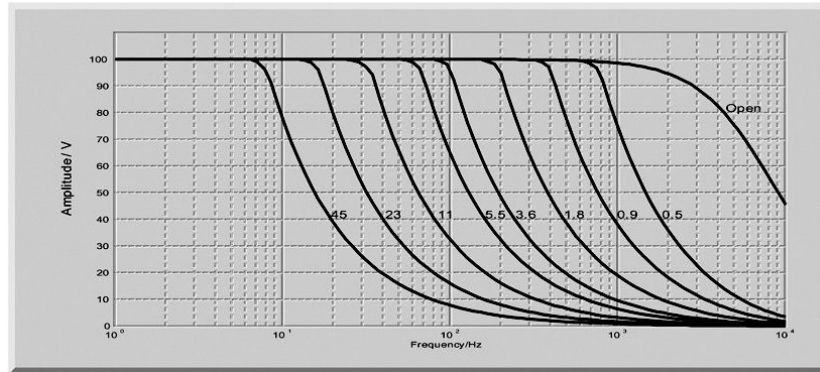
Fig. 2-13 Response Curve of the E-663 piezo amplifier.
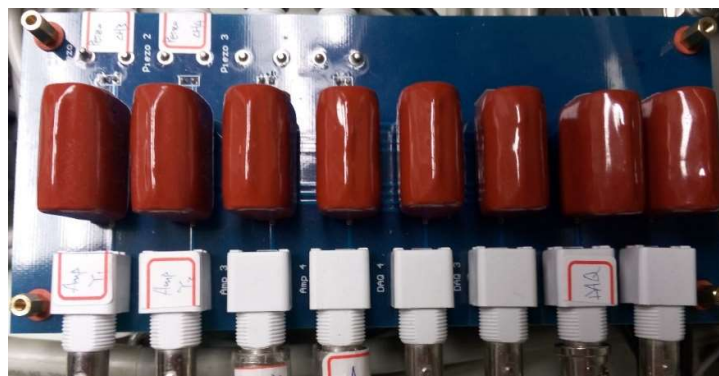
Fig. 2-14 External capacitor for charge measurement.

2.3.2 Software-hardware integration

The Fig. 2-15 shows what happened during one loop period. The sampling time is 5 kHz so the time length is $20\mu s$. The loop of control process is triggered by the rising edge of the sampling clock of the DAQ board. There are in total three stages included in one loop: data reading, control signal calculating and input writing.

During the data reading stage, the syntax"DAQmxReadAnalogF64" is processed initially and the DAQ board starts to collect data saved in the buffer (i.e., voltage drop of the capacitor) for later use. In this function, the DAQ board converts the analog output (voltage) into digital signal so that the data get from buffer is newly measured. Except for the data from DAQ board, the measurement data will be obtained as well from the function called syntax "N1231AGetRawPosVel" that is executed next.

15

`

Next stage is the control signal calculating stage, which means all processes related with the calculation of control signal is done in this stage including error calculation, controller realization and hysteresis compensation. When the calculation of the control signal is brought to an end, the program will proceed to the last stage, input writing.

In final stage, the PC firstly writes the calculation results obtained from last stage. In the later chapter we can see that to drive plant of one axis, there are two voltages data needed. So the data can be different due to different control needs but they are driven to plant together in this stage. After all functions performed, the program waits until the current clock cycle finished by executing syntax "DAQmxWaitForNextSampleClock".
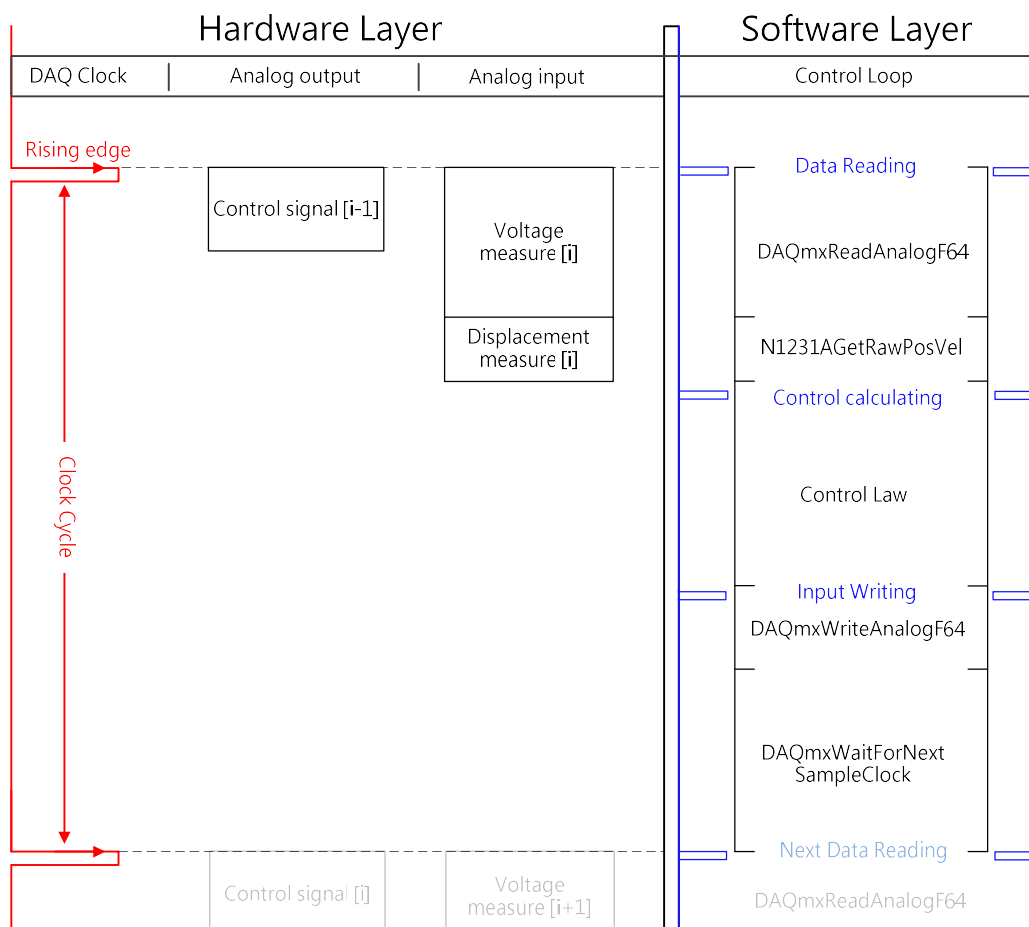
Fig. 2-15 Hardware-software integration

16

Chapter 3   Hysteresis Description
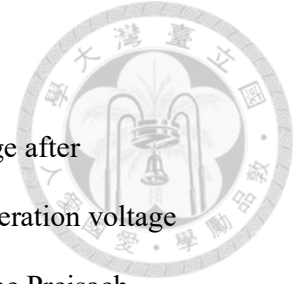
Due to Hysteresis phenomenon, the relationship between the voltage after compensation which also actually derived to stage and the voltage of operation voltage is nonlinear. In this thesis, the hysteresis nonlinearity is formulated by the Preisach model[4] which is commonly used now.

In this chapter, firstly Hysteresis operator is defined to describe Hysteresis phenomenon, whose characters are shown in section 3.2, and then the Preisach model including both physical and mathematical expression are introduced, and a simplified polynomial Preisach model used is discussed in detail. The actual process of parameters' identifications local at next chapter.

3.1   Hysteresis operator

Hysteresis operator is defined as the function of charge q flowing through the piezo-actuator. It is represented as

$$u_h = H(q) \tag{3.1}$$

Since the hysteresis operator can be described as the function of charge q, hysteresis voltage u_h is regarded as the energy consumption of the input voltage u and the remaining voltage u_{remain} applied to the system is defined as

$$u_{remain} = u - H(q) = u - u_h \tag{3.2}$$

3.2   Hysteresis phenomenon

In this section, different type of input signals are feed to system to show the different Hysteresis phenomena.

`

3.2.1 Hysteresis phenomena under signals of different frequencies.

The input signals are all sinusoid wave with magnitude of 2.5V, but the frequency varies to 10, 30, 60, 100 and 200Hz. When the system is operated under those input signals, the hysteresis between u and u_{remain} is as shown in Hysteresis operator
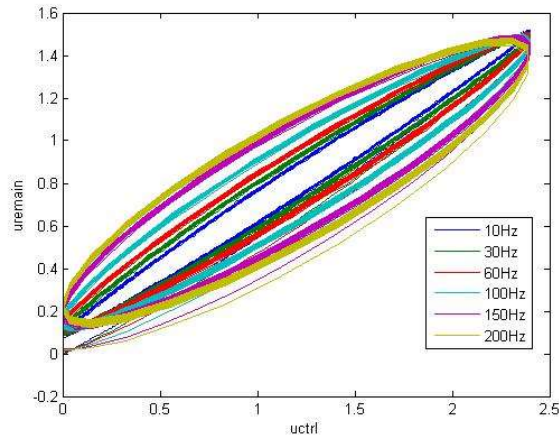
Fig. 3-1 Hysteresis phenomena of signals under different frequencies

It can be concluded that the Hysteresis phenomenon is getting more obvious with the increasing of frequency of input signal.

3.2.2 Hysteresis phenomena under signals of different velocities.

It is defined that the velocity of the signal is the voltage change per second. The input signals are zigzag with maximum magnitude 2.5V as well and the velocities of those signals are 10V/s, 50V/s, 100V/s, and 200V/s. The plot of the hysteresis phenomena under different operation velocity is shown in Fig. 3-2.

18
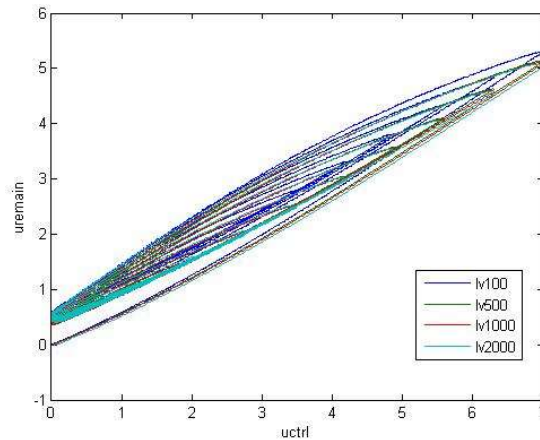
Fig. 3-2 Hysteresis phenomena of zigzag signals under different velocities

3.3   Preisach Model of Hysteresis

3.3.1   Model Description

The Preisach model originated from a hypotheses related to the magnetization phenomenon and is thought as a physical model of hysteresis. The hypothesis is that the hysteresis phenomenon can be described as the construction of backlash operators $\hat{\gamma}_{\alpha\beta}$ [4].

The relationship between input and output of backlash operator $\hat{\gamma}_{\alpha\beta}$ is shown in Fig. 3-3, where u is the input voltage and (α, β) are the switching thresholds of ascending and descending operation. The operator output is either 0 or 1, depending on the operating condition and the input voltage. When the input u is rising, the operator is in the ascending operation and the output will remain as 0 unless u surpass the rising threshold α. While in the descending operation, the operator output will remain as 1 before u is lower than the falling threshold β. The operating principle is shown in Fig. 3-3-(b) and (c).

19

(a)　　　　　　　　　(b)　　　　　　　　　(c)
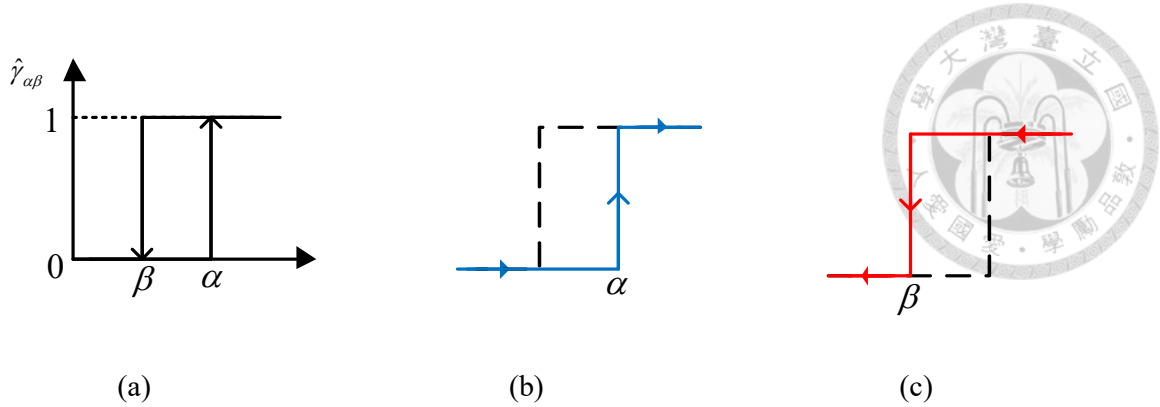
Fig. 3-3 (a) Backlash operator, (b) Ascending operation, (c) Descending operation

The hysteresis phenomenon is modeled as a combination of infinity backlash operators, and each backlash operator is weighted by a density function $\mu(\alpha,\beta)$, as depicted in (3.3). The corresponding mathematical expression [5][6] is defined as

$$P(u) = \iint\limits_{\alpha \geq \beta} \mu(\alpha,\beta)\hat{\gamma}_{\alpha\beta}\big[u(t)\big]d\alpha d\beta \tag{3.3}$$

where $P(u)$ is the output of Preisach model, $\mu(\alpha,\beta)$ is the density function, and $\hat{\gamma}_{\alpha\beta}$ is the backlash operator. This equation corresponds to the weighted integration of the area S^+ in Fig. 3-5-(a).
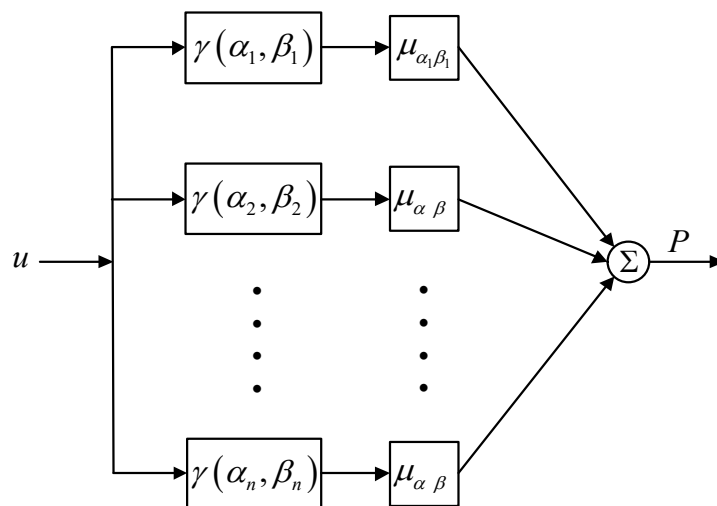
Fig. 3-4　Parallel connection of infinity weighted backlash operators

20

As described in Equation (3.3), the operating process is shown in Fig. 3-5 . The α axis and β axis represent the ascending and descending operation respectively. The operating point of this model is always on the 45 degree line($\alpha = \beta$) during both ascending and descending operation. During the inactive state, the operating point will remain on the point $\alpha = \beta = 0$.
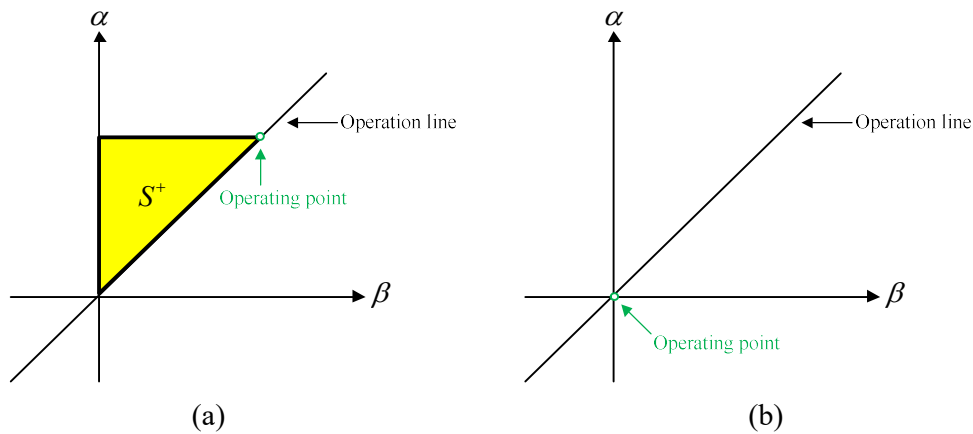
Fig. 3-5 (a) Preisach integration area and operating point, (b) Preisach integration area when piezo is in inactive state.

When the piezo stage is stimulated from inactive state ascending to α_1 under driving voltage, the operating point will move along the operating line to the point $\alpha = \alpha_1$ and the integration area is the area in α axis, operating line and the line $\alpha = \alpha_1$ as shown in Fig. 3-6. Similarly, when there is a decrease in driving voltage from α_1 to β_1, the position of the operating point will also decrease as well. The integration area now is a quadrilateral bounded with α axis, operating line and the line $\alpha = \alpha_1$ plus $u = \beta_1$ axis. This is illustrated in Fig. 3-7.

21
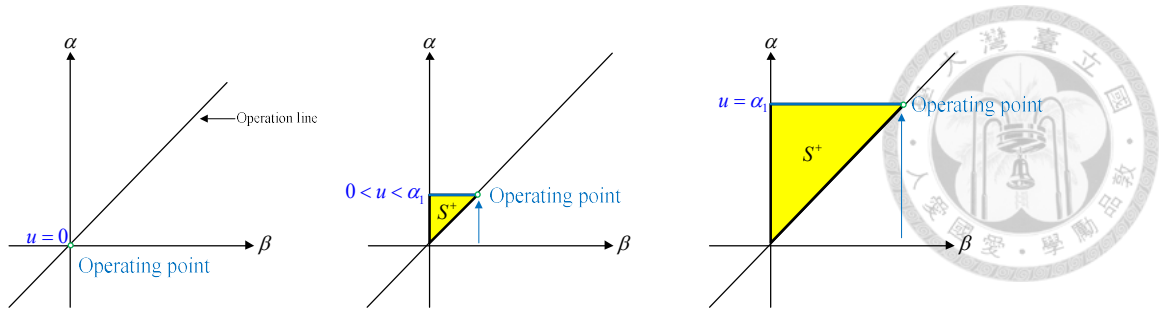
Fig. 3-6 Integration area variation from $u=0$ to $u=\alpha_1$
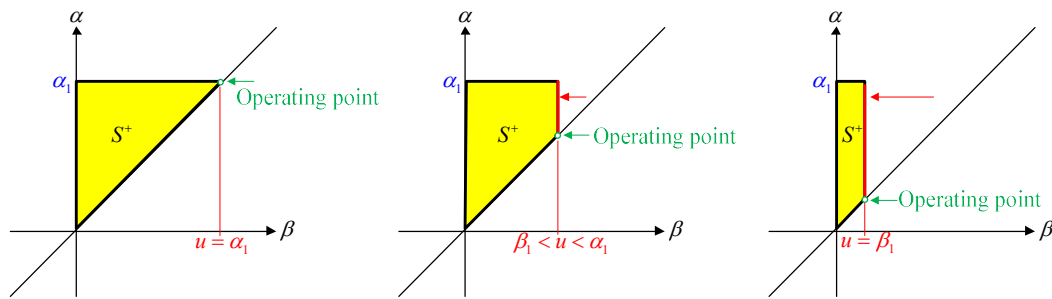
Fig. 3-7 Integration area variation from $u=\alpha_1$ to $u=\beta_1$

Similar to the previous operation, if the operating voltage is raised to α_2 again and then lowered to β_2 as shown in Fig. 3-8, the change of integration area now adds another quadrilateral bounded with α axis, operating line and the line $\alpha=\alpha_2$ plus β $=\beta_2$ axis as it is shown in Fig. 3-9. This process is called hysteresis congruency, which saying that the area variations are identical during two process goes through the same amount of voltage change. Since the area differences are the same, the hysteresis phenomena are equivalent.

22
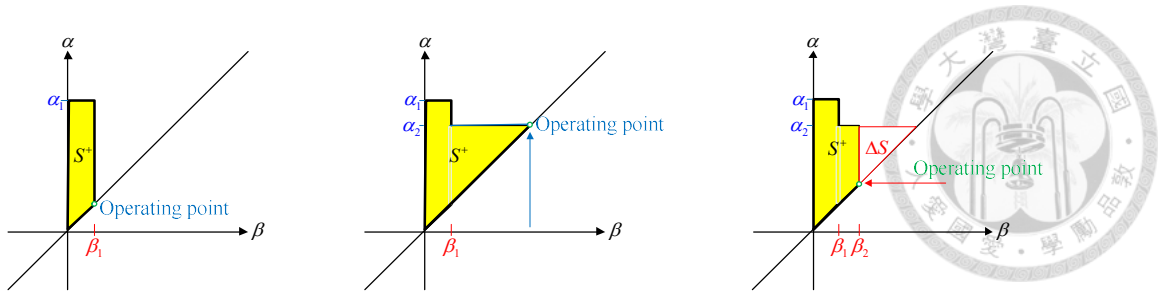
Fig. 3-8 Continued operation, u rises to α_2 and then descends to β_2
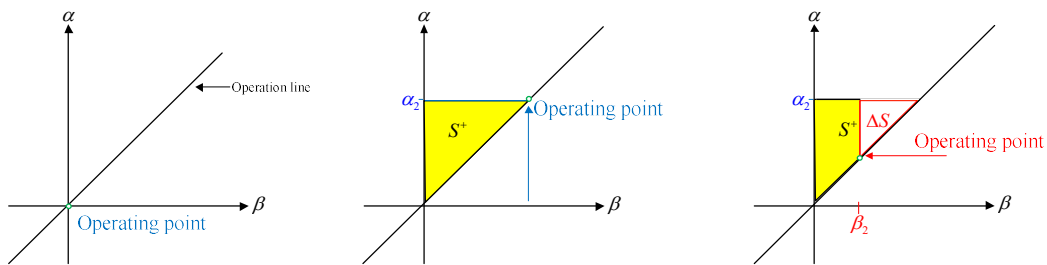
Fig. 3-9 Direct operation, u rises to α_2 and then descends to β_2 directly

In the condition that the operating voltage exceeds either the local maximum or the local minimum of the previous operating process, the recorded hysteresis of the previous operation will be totally canceled. This property is named as the wipe out property .The following example illustrates the procedure of the property.
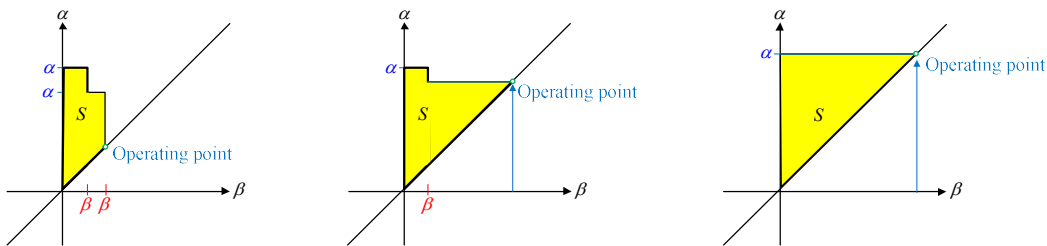
Fig. 3-10 Wipe Out Property of hysteresis

Fig. 3-10 also indicates that both of the integration area and the resulting hysteresis are total the same no matter the operation voltage ascents from β_2, and reach α_3 after exceeding α_2 and α_1 or the operation voltage goes from zero to α_3 directly.

23

3.3.2 Preisach Model

(a)   (b)
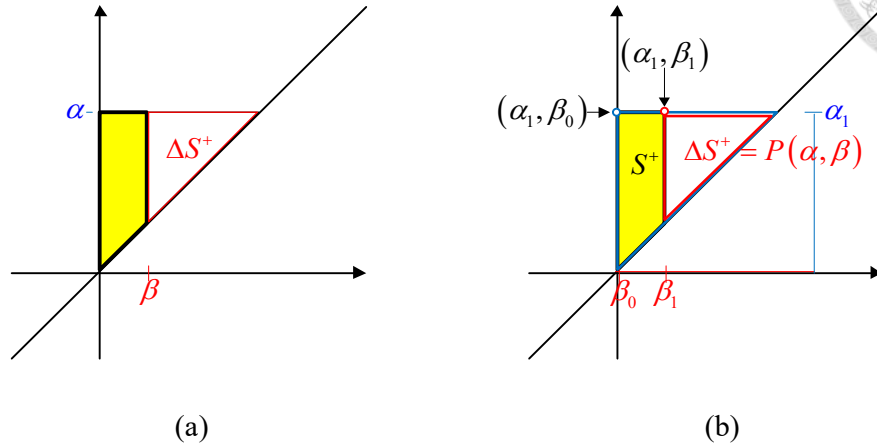
Fig. 3-11 The result of hysteresis described by Preisach model. (a) hysteresis variation

$$\Delta S^+ = P(\alpha, \beta), \text{ (b) resulting hysteresis } S^+ = P(\alpha_1, \beta_0) - P(\alpha_1, \beta_1)$$

The meaning of the mathematical model is that if the input u ascends to α_i and then

descends to β_i, the hysteresis difference during the descending procedure is $P(\alpha_i, \beta_i)$.

Moreover, this function can also be used to find the integral result over the trapezoid

area; in Fig. 3-11-(b), for example, the trapezoid area is equal to the larger triangular

area $P(\alpha_1, \beta_0)$ minus the smaller triangular $P(\alpha_1, \beta_1)$. Since the variation of S^+

must satisfy the operating condition as defined in Fig. 3-6, Fig. 3-7 and Fig. 3-10.

Referring to Fig. 3-12 , the integral region must be the combination of different

triangular regions. The Preisach integration area can be calculated by

$$F(u) = \sum_{i=1}^{n} \left\{ P(\alpha_i, \beta_{i-1}) - P(\alpha_i, \beta_i) \right\} \tag{3.5}$$

24
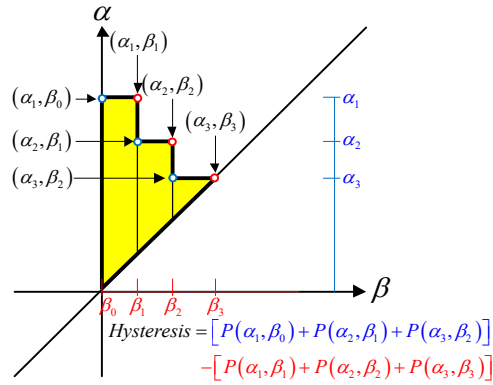
Fig. 3-12 Hysteresis calculation using Preisach integration area

3.3.3 Polynomial Preisach model

A polynomial expression for Preisach model was suggested by Wen et al[36]. It is assumed that the higher order of the Preisach polynomial results to better model accuracy. However, this will also increase the calculation time. To compromise between the accuracy and the calculation time, the order of the Preisach polynomial is chosen to be four, and thus the corresponding Preisach polynomial is formulated as

$$
\begin{aligned}
F(\alpha,\beta) &= \sum_{j=0}^{4-i}\sum_{i=0}^{4} C_{ij}\alpha^i\beta^j \\
&= C_{01}\alpha + C_{10}\beta + C_{11}\alpha\beta + C_{20}\alpha^2 + C_{02}\beta^2 + \cdots
\end{aligned}
\tag{3.6}
$$

where $[C_{01}, C_{10}, \dots, C_{04}]$ are the identification target.

Chapter 4　　System Description
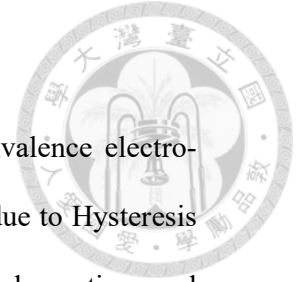
This chapter will cover the mechanical structure as well as equivalence electro-Mechanical Model of the piezo-actuated system including decoupling due to Hysteresis phenomena which will be discussed detailed in Chapter 4, the mechanical equations and parameters identification corresponding to the hardware structure.

4.1　　　Mechanical Structure

When only the x-direction is considered, the overall structure can be simplified as shown in Fig. 4-1. The equivalent structure can also be represented as shown in Fig. 4-2.
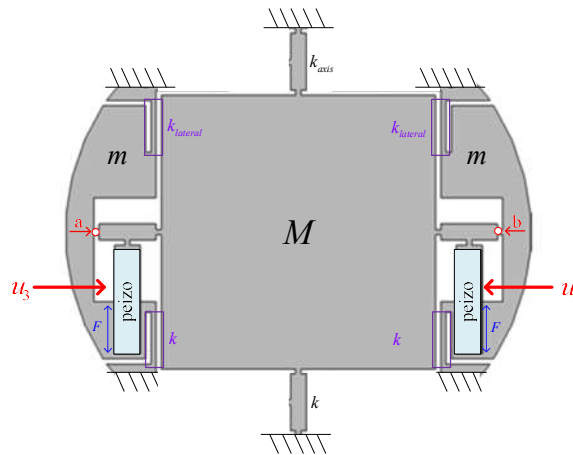
Fig. 4-1 The simplified structure where only x-axis is considered[35]

Point a and point b can be regarded as stationary because the spring constant k_3 is much greater than k_1, the elongation of the equivalent spring on both sides are negligible. The relationship between the stage displacement y in center and the piezo elongation Δ_p which happens only one side can thus be formulated as:

$$\Delta_p = 0.5y \tag{4.1}$$
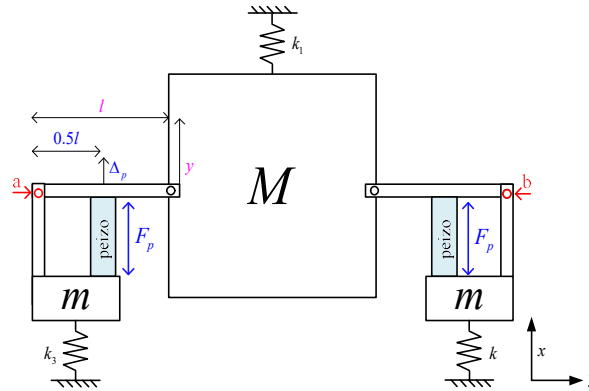
Fig. 4-2 Equivalent structure of flexure-hinge stage

4.2 Electro-Mechanical Model of Piezo-actuated System

This section includes the electromechanical model of the piezo actuator, with the help of system decoupling, the relationships between variables are derived.

4.2.1 Piezo-actuator model

The piezo-actuator model is an electromechanical model of consists of two different models, the electrical model and a mechanical model[15], also called Voltage transformation model. In the electrical model, u represents the voltage applied on the experimental stage. In the stage, the voltage drop is absorbed by two components, firstly hysteresis operator $H(q)$ with the amount of u_h, and the stage equivalent capacitance c_p with the amount of $u_p = u - u_h$. The parameters of this equivalent capacitance are connected to the mechanical model by the constant T_{em} which represents the transformation ratio of the electromechanical transducer. This parameter T_{em} can actually be separated into two transformation ratios with same values. One transformation maps voltage u_p to force generation F_p, and the other correlates the elongation y to

27
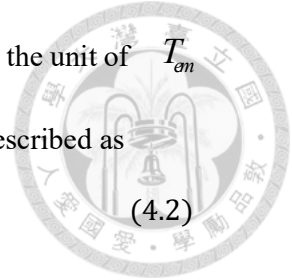
charge q_p. So the relations are $F_p = T_{em}u_p$ and $q_p = T_{em}y$. Therefore, the unit of T_{em}

can either be N/V or C/m. The dynamic equation of the system can be described as

$$F_p - F_{ext} = M_p\ddot{y} + B_p\dot{y} + K_py \tag{4.2}$$

Where F_{ext} is the externally applied force. M_p, B_p, K_p are the mass, damping

constant and spring constant of the piezo actuator respectively.
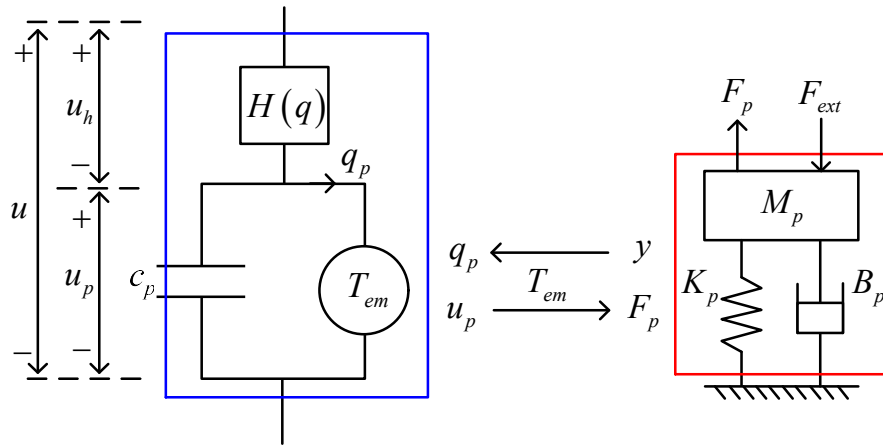
Fig. 4-3 Electromechanical model of piezo actuator.

The mechanical model can be approximated by a mass-spring-damper system and

the combined mechanism can be regarded as a second-order mass-spring-damper system.

The governing equation is modified as

$$\begin{cases} F_p - F_{ext} = M_p\ddot{y} + B_p\dot{y} + K_py \\ M = M_s + \frac{4M_p}{\pi^2} \\ B = B_s + B_p \\ K = K_s + K_p \end{cases} \tag{4.3}$$

where (M_s, B_s, K_s) and (M, B, K) represent the mass, damping constants, and spring

constants of the piezo stage and the overall system, respectively.

4.2.2 The equation of transformation ratio

As it is shown in Fig. 4-4, in this thesis, the structure of the piezo actuator proposed

is slight changed in order to measure the change which is the same as the system proposed

28

by L.S. Chen *et al.* [16]. An additional real capacitor with capacitance c_e as introduced in chapter 2 is connected to the piezo to measure the total charge in the actuator, since the current flowing through the actuator is same as the current flow through the added capacitor. The total charge flowing through the piezo-actuator can be calculated by measuring the voltage drop V_e on the capacitor connected to it.
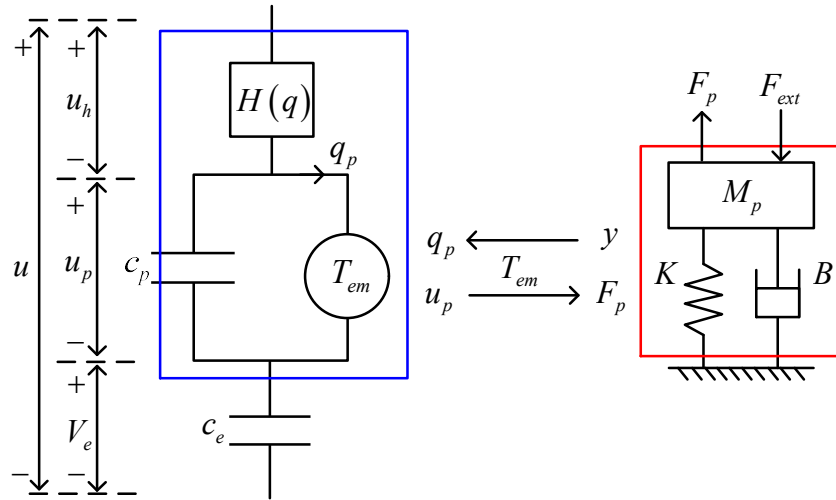
Fig. 4-4 Modified Electromechanical model of piezo actuator

From the electromechanical model of the piezo actuator [15], the force generated by the piezo-actuator is

$$F_p = T_{em}u_p = \Gamma\Delta_p \tag{4.4}$$

Where Γ is the stiffness of the piezo-actuator. The charge stored in the electromechanical transducer (Q_T) can be described as

$$Q_T = T_{em}\Delta_p \tag{4.5}$$

The overall charge stored in piezo-actuator is equal to the sum of the charge in the equivalent capacitor (Q_p) and the charge in the transducer as it is shown below.

$$q = c_eV_e = Q_p + Q_T = c_pu_p + T_{em}\Delta_p \tag{4.6}$$

29
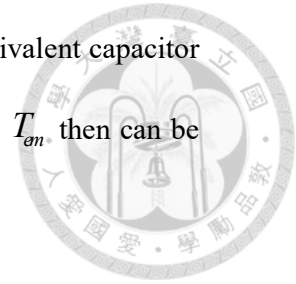
The value of stiffness Γ will be estimated in next section and the equivalent capacitor c_p are known by measurement. The equations of transformation ratio T_{em} then can be calculated by combining the Equation(4.4) (4.5) and (4.6)

$$T_{em}^2 - \left(\frac{q}{\Delta_p}\right)T_{em} + \Gamma c_p = 0 \tag{4.7}$$

Where q and Δ_p are the measured value of both the charge and elongation respectively. Besides, from Equation (4.6) a, u_p is obtained as

$$u_p = \frac{\left(C_e V_e - \Delta_p T_{em}\right)}{c_p} \tag{4.8}$$

The hysteresis voltage u_h can be calculated

$$u_h = u - u_p - V_e \tag{4.9}$$

(a)   (b)
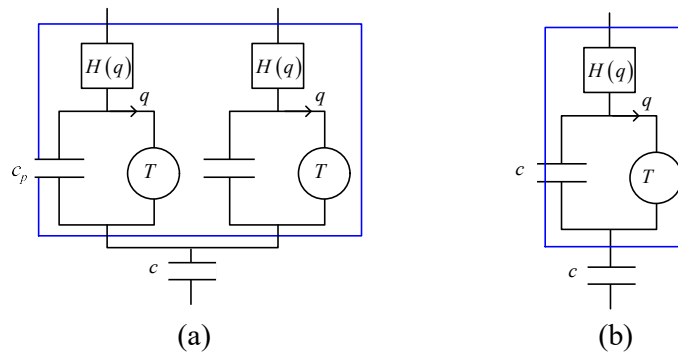
Fig. 4-5 Parallel connected piezo-actuator model. (a) Original structure (b)Single-piezo equivalent structure

Since the structure of each piezo-actuator is identical, the two units are connected in parallel, and the difference of two u nits are neglected because they are the same with each other, the parameters of the equivalent structure can be doubled as listed following:

30

$$T_{em2} = 2T_{em}$$
$$C_{p2} = 2c_p$$

(4.10)

Equation (4.9) implies that the transformation ratio T_{em2} is two times the value of the original piezo-actuator. For while the stage is operated under the same amount of voltage, the force is generated by two piezo-actuators. At the same time, the stiffness Γ is doubled. The modified equation becomes

$$\begin{cases} F_p = 2T_{em}u_p = 2\Gamma\Delta_p \\ q = c_eV_e = 2c_pu_p + 2T_{em}\Delta_p = 2c_p\dfrac{\Gamma\Delta_p}{T_{em}} + 2T_{em}\Delta_p \end{cases}$$

(4.11)

Thus the equation to estimate T_{em} is obtained as

$$T_{em}^{2} - \left(\frac{q}{2\Delta_p}\right)T_{em} + \Gamma c_p = 0$$

(4.12)

4.3   Parameter ID

In equation(4.2), except for T_{em}, the only parameters that required to know is Γ

4.3.1   Estimation of the Equivalent Stiffness

Parameter Γ is the equivalent stiffness of the stage when the force is applied on the piezo. It is only related to the geometry and stiffness of the mechanical stage, thus Γ can be obtained by simulation environment in ANSYS. The force generated by each piezo is set to be 150N, which causes the elongation of the piezo to be $1.663\ \mu m$. The overall Γ is then estimated as $90.2\ N/\mu m$. The simulation results are shown in Fig. 4-6.
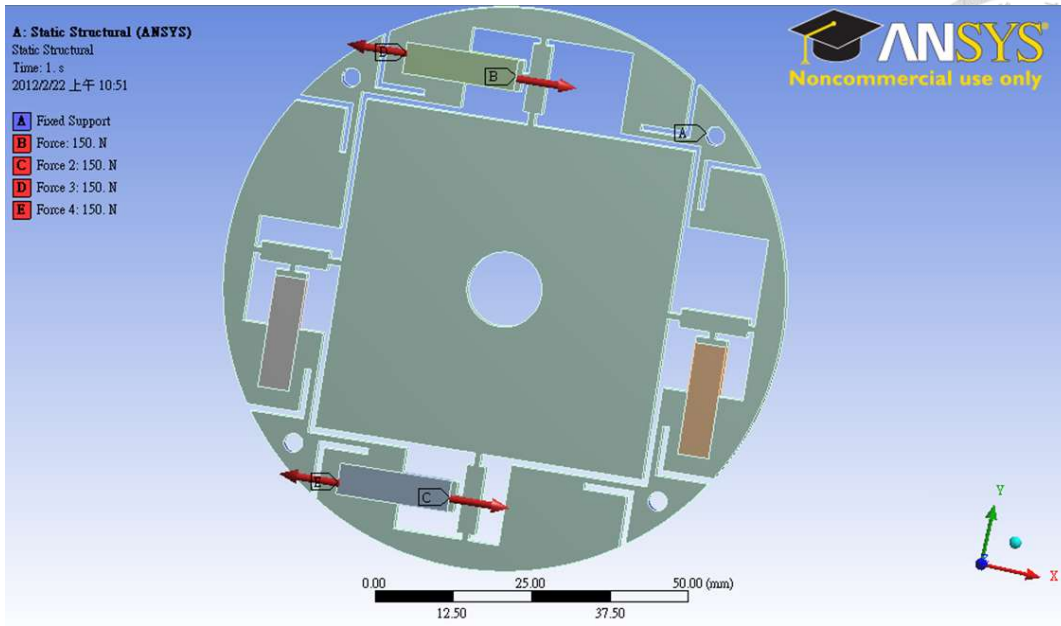
(a) The applied force generated by the piezo.
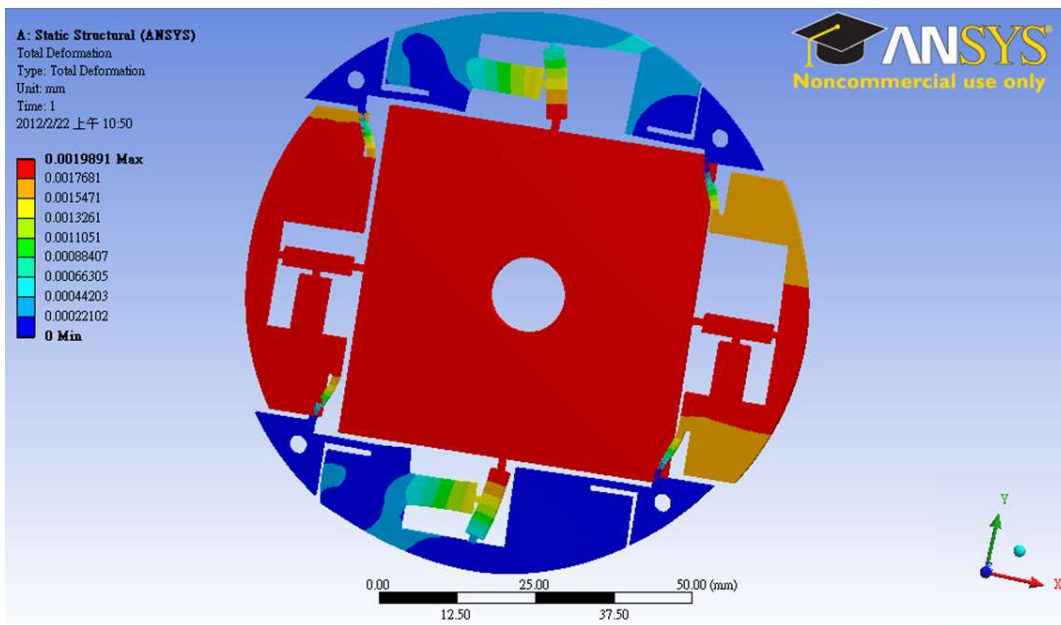
(a) The resulting deformation of the stage

Fig. 4-6 The static force simulation in ANSYS. (a) Force applied (b) Deformation

4.3.2 Identification of the transformation ratio

An experiment based on the equation $T_{em}^2 - \left(q / 2\Delta_p \right) T_{em} + \Gamma c_p = 0$ is carried out to know the transformation ratio T_{em}. Because both the damping ratio and stage mass are not involved, this experiment is operated with a slow-speed ramp signal. The displacement y can be measured by laser path so the Δ_p is obtained due to $\Delta_p = 0.5y$ and the charge q, which is stored in the capacitor can be measured by as well. In Fig. 4-7, the relationship between the input voltage u and the stage displacement y is shown. While Fig. 4-8 shows the relationship between the charge stored in the capacitor, which is equivalent to the charge passing through the piezo-actuator and the displacement y.
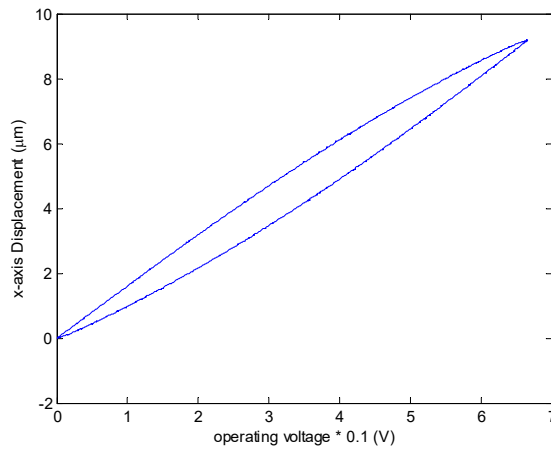
Fig. 4-7 Relationship between operating voltage and stage displacement

`
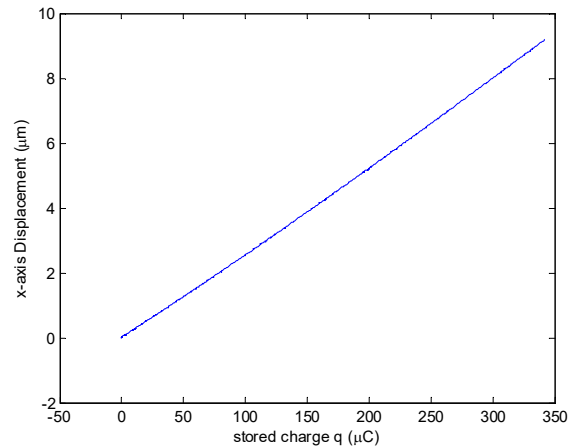
Fig. 4-8 Relationship between piezo stored charge and stage displacement

In the equation $T_{em}^2 - \left(q / 2\Delta_p\right)T_{em} + \Gamma c_p = 0$, the value of c_p and c_e are 1.8 and 84 respectively. the value of $q / \left(2\Delta_p\right)$ is calculated from the Least-Square method, finially the value of T_{em} is calculated as 4.95 and 32.81 (unit N/V or C/m). In order to verify these two solutions, Equations (4.3) and Equations (4.8) are used to obtain the corresponding u_h and u_p. By increasing the input voltage u, the operation voltage u_p and the hysteresis consumption u_h are expected to increase. According to Fig. 4-9 and Fig. 4-10, only the result calculated by T_{em}=4.95 satisfies the assumption, thus T_{em} is suggested to be 4.95.
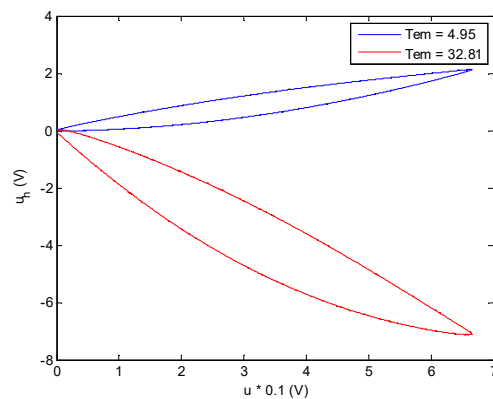
Fig. 4-9 Relationship between operating voltage u and hysteresis voltage u_h

34
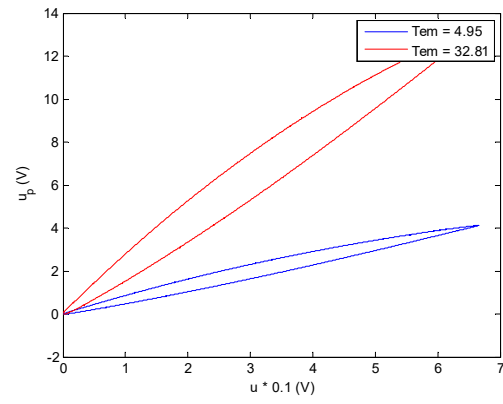
Fig. 4-10 Relationship between operating voltage u and force generating voltage u_p

Chapter 5　System ID
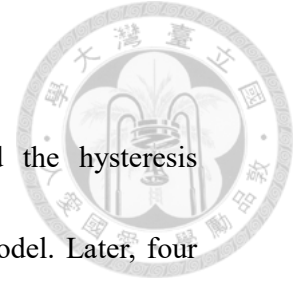
In this chapter, firstly the force generating voltage u_p and the hysteresis consumption u_h can be estimated by 4-order polynomial Preisach model. Later, four stage transfer functions of operating voltages with two in same direction and different direction axis can be further identified. The identification of hysteresis phenomenon is required for constructing the Hysteresis model while the controller design is based on system identification.

5.1　Hysteresis ID

As introduced in Chapter 4, the hysteresis phenomenon is normally used to describe the nonlinear relationship between the input voltage u and the output displacement y.

In this section, the main content is to introduce the identification process of the hysteresis phenomenon.

As said, the 4-order polynomial expression for Preisach model was proposed by Wen et al[32].

$$
\begin{aligned}
F(\alpha,\beta) &= \sum_{j=0}^{4-i}\sum_{i=0}^{4} C_{ij}\alpha^i\beta^j \\
&= C_{01}\alpha + C_{10}\beta + C_{11}\alpha\beta + C_{20}\alpha^2 + C_{02}\beta^2 + \cdots
\end{aligned}
\tag{5.1}
$$

As in chapter 4, the hysteresis variation $P(\alpha,\beta)$ can be estimated, both α and β are directly decided by the operating voltage u

In order to identify the coefficients in Equation(5.1), a low-speed zigzag signal as illustrated in Fig. 5-1 is used to drive the piezo-actuator. The resulting displacement y and operating charge q can be simultaneously recorded for calculation.

Given by the experimental data, the relationship between u and u_h can be written

36

`

as

$$F(\alpha,\beta)=C_{01}\alpha+C_{10}\beta+C_{11}\alpha\beta+C_{20}\alpha^2+C_{02}\beta^2+\cdots$$
$$\rightarrow \Delta h_{ij}=C_{01}u_{i0}+C_{10}u_{ij}+C_{11}u_{i0}u_{ij}+C_{20}u_{i0}^2+C_{02}u_{ij}^2+\cdots \tag{5.2}$$
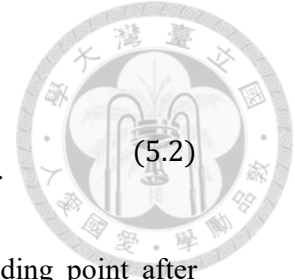
where u_{i0} is the i-th local maximum of u, u_{ij} is the j-th descending point after

ascended to u_{i0}, and Δh_{ij} is the hysteresis variation during the operation. Thus, all the

equations according to Equation (5.2) can be rearranged in matrix expression as

following

$$
\begin{bmatrix}
u_{10} & u_{11} & u_{10}u_{11} & u_{10}^2 & u_{11}^2 & \cdots \\
u_{10} & u_{12} & u_{10}u_{12} & u_{10}^2 & u_{12}^2 & \cdots \\
u_{10} & u_{13} & u_{10}u_{13} & u_{10}^2 & u_{13}^2 & \cdots \\
& & \vdots & & & \\
u_{i0} & u_{ij} & u_{i0}u_{ij} & u_{i0}^2 & u_{ij}^2 & \cdots \\
& & \vdots & & &
\end{bmatrix}
\begin{bmatrix}
C_{01} \\ C_{10} \\ C_{11} \\ \vdots \\ \vdots \\ C_{04}
\end{bmatrix}
=
\begin{bmatrix}
\Delta h_{11} \\ \Delta h_{12} \\ \Delta h_{13} \\ \vdots \\ \Delta h_{ij} \\ \vdots
\end{bmatrix}
\tag{5.3}
$$

which satisfies the linear equation form

$$AX = B \tag{5.4}$$

where

$$
A=
\begin{bmatrix}
u_{10} & u_{11} & u_{10}u_{11} & u_{10}^2 & u_{11}^2 & \cdots \\
u_{10} & u_{12} & u_{10}u_{12} & u_{10}^2 & u_{12}^2 & \cdots \\
u_{10} & u_{13} & u_{10}u_{13} & u_{10}^2 & u_{13}^2 & \cdots \\
& & \vdots & & & \\
u_{i0} & u_{ij} & u_{i0}u_{ij} & u_{i0}^2 & u_{ij}^2 & \cdots \\
& & \vdots & & &
\end{bmatrix}, \quad
X=
\begin{bmatrix}
C_{01} \\ C_{10} \\ C_{11} \\ \vdots \\ \vdots \\ C_{04}
\end{bmatrix}, \quad
B=
\begin{bmatrix}
\Delta h_{11} \\ \Delta h_{12} \\ \Delta h_{13} \\ \vdots \\ \Delta h_{ij} \\ \vdots
\end{bmatrix}
\tag{5.5}
$$

Noting that the row dimension of matrix A is larger than the column-dimension. In order

to solve X, Least-Square method is implemented as indicated in the following

$$X = \left(A^T A\right)^{-1} A^T B \tag{5.6}$$

where the solution of A satisfies

37

`

$$\|AX - B\| \le \|AX_{other} - B\| \quad \forall \, X_{other} \tag{5.7}$$

According to Fig. 3-2, it is implies that with higher velocity, the hysteresis phenomenon of the zigzag signal becomes greater. Using the obtained Preisach polynomial function by giving a zigzag signal with velocity = 1500, the simulated hysteresis consumption is compared with the real hysteresis as shown in Fig. 5-2.
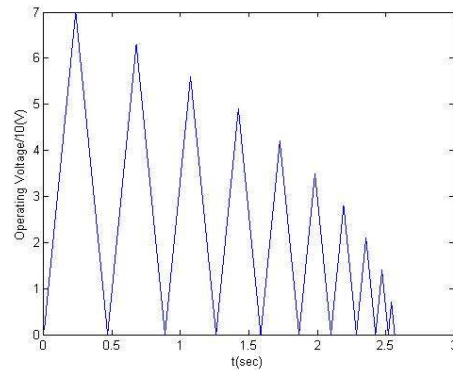
Fig. 5-1 Input signal for Preisach model identification.
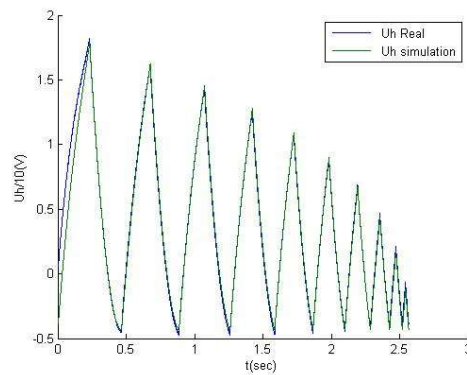
Fig. 5-2 (a)Hysteresis voltage u_h estimated by Equation (4.9)

5.2 System ID

This section is divided three parts .The first part introduces the four functions that will be identified from physical relationship and then both the notification and the input

38

`

signal processed into system. The result is presented in the third part.

5.2.1 System Decoupling

Supporting the measured results of the Path A and Path B in Fig. 5-2 are different, which means the stage is not running in parallel. As shown in, suppose there are two axis named 0 and 1. When one side pushing, it will not only affect the side itself, but also the other side.
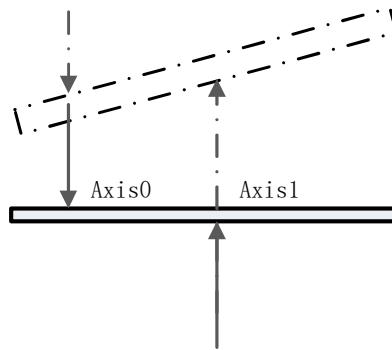
So when the stage is pushed, the measured value contains two part: the impact of the actuators in same side which is main factor and the impact of the actuators in other side.

$$\begin{bmatrix} y_0 \\ y_1 \end{bmatrix} = \begin{bmatrix} G_{00} & G_{10} \\ G_{01} & G_{11} \end{bmatrix} \begin{bmatrix} u_0 \\ u_1 \end{bmatrix} \tag{5.14}$$

So in total there are four functions G_{00}, G_{01}, G_{10}, and G_{11} that need to be identified

5.2.2 Preparation of System Identification

To finish the ID process, an input signal need to be chosen to get a best result. The requirement including that firstly it can covers all frequency that need to be formulated, secondly, it will cause a response that should be safe that will not do damage to experiments stage. What's more, It would be better that it is easy to implement. A chirp signal and a step signal are combined to be the input voltage to stimulate the dynamic characteristics of the stag. Since the operation is mainly under lower frequencies, the

exponential chirp is chosen. The input signal $u(t)$ is

$$u(t) = A + A\sin\left[2\pi f_0\left(\frac{k^t - 1}{\ln(k)}\right) + \phi_0\right] \qquad (5.15)$$

where A is the amplitude of both the step and the chirp signal, f_0 is the initial frequency, k is the increasing rate of frequency of the chirp signal. The step signal and the phase shift $\phi_0 = 1.5\pi$ are used to move the range of the input voltage from $[-A, A]$ to $[0, 2A]$ since piezo-actuators behaves more consistently under positive voltage input in general conditions. The frequency of the chirp signal is

$$f(t) = f_0 \times k^t \qquad (5.16)$$

Since the resonant frequency of the stage was estimated to be around 900Hz from former experiments [35], the frequency of the chirp signal is chosen to start from 0.5 to 1000Hz. A is chosen to be 1.5 (V). The corresponding equation of the input signal is

$$u(t) = 1.5 + 1.5\sin\left[2\pi \times 0.5\left(\frac{k^t - 1}{\ln(k)}\right) + \frac{3}{2}\pi\right] \qquad (5.17)$$

The frequency growing rate k is defined as

$$k = \left(\frac{f_{end}}{f_o}\right)^{1/t_{end}} \qquad (5.18)$$

where f_{end} is the end frequency (1000Hz), f_0 is the initial frequency (0.5Hz) and t_{end} is the end time (0.5s) of the chirp signal. To emphasize the performance under low frequency signal, a low pass filter with corner frequency at 300Hz is implemented to modify the input signal as following

$$L(s) = \frac{2\pi \times 300}{s + 2\pi \times 300} \qquad (5.19)$$

40
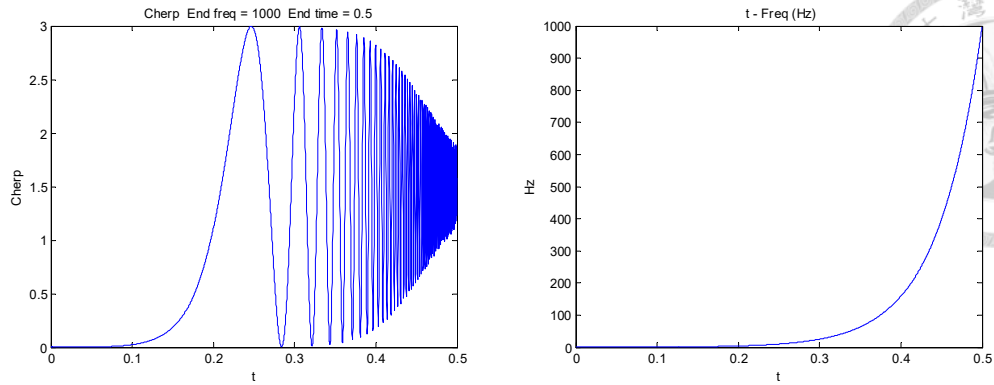
Fig. 5-3 (a)Chirp signal from 0.01 to 1000 Hz   (b)Frequency change with time

5.2.3   Identification Results

Compared with operating input u , the force-generating voltage u_p as the effective input voltage of the stage ,is a better choice ,because the relationship between operating input u and output displacement y is affected by the hysteresis, and as the value of T_{en} is identified, it is able to estimate the force-generating voltage u_p by Equation (4.9). In consequence, the stage transfer function   can be obtained by system ID technique.

By the N4SID method which belongs to the System Identification Toolbox in MATLAB [29][30], the transfer function of the system is estimated as

$$G_{00} = \frac{5.7512\ z^{\wedge}-1\ (1-z^{-1})\ (1+0.058\quad^{-1})}{(1+0.8532z^{-1})\ (1-z^{-1})(1\ -\ 0.5537z^{-1}\ +\ 0.739\quad^{-2})} \qquad (5.20)$$

$$G_{01} = \frac{1.263\quad^{\wedge}-1\ (1-z^{-1})\ (1+0.6407z^{-1})}{(1+0.9787z^{-1})\ (1-z^{-1})(1\ -\ 0.7255z^{-1}\ +\ 0.9298z^{-2})} \qquad (5.21)$$

$$G_{11} = \frac{4.6959z^{\wedge}-1\ (1-z^{-1})\ (1+0.3285z^{-1})}{(1+0.8939z^{-1})\ (1-z^{-1})(1\ -\ 0.6526z^{-1}\ +\ 0.7147z^{-2})} \qquad (5.22)$$

$$G_{01} = \frac{1.2634\ ^{\wedge}-1\ (1-z^{-1})\ (1+0.6407z^{-1})}{(1+0.9787z^{-1})\ (1-z^{-1})(1\ -\ 0.7255z^{-1}\ +\ 0.9298z^{-2})} \qquad (5.23)$$

With fatting rates are 93%, 95%, 90% and 94% respectively.

41

Chapter 6　　Control Method

　　The control structure in this thesis is shown in Fig. 6-1, which can mainly split into three parts, first one is hysteresis linearization control, second one is synchronizing control, and final part is tracking control
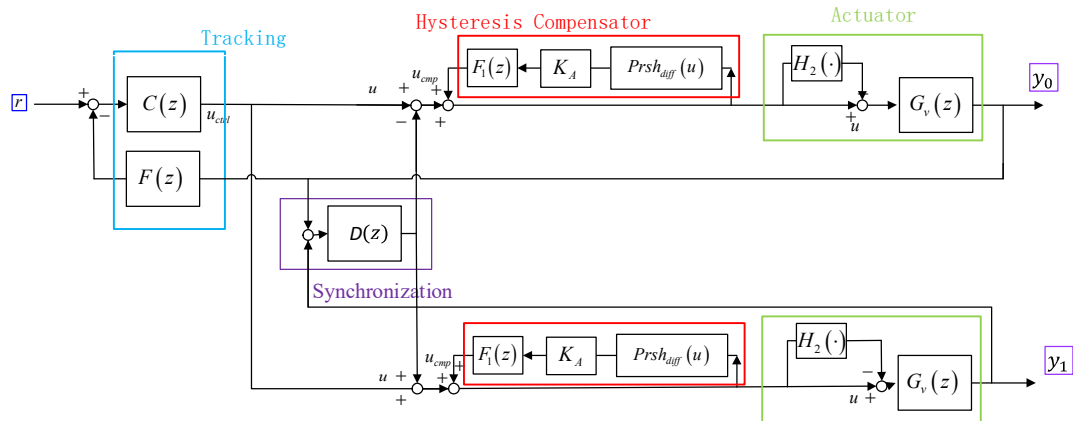
Fig. 6-1 Overall control structure

6.1　　The inner loop control

　　The inner loop is designed to linearize the hysteresis phenomenon, contains a hysteresis observer and compensator, as shown in Fig. 6-1. If the inner loop works perfectly, the hysteresis phenomenon will be totally eliminated. The structure will then become simpler as shown in Fig. 6-2.
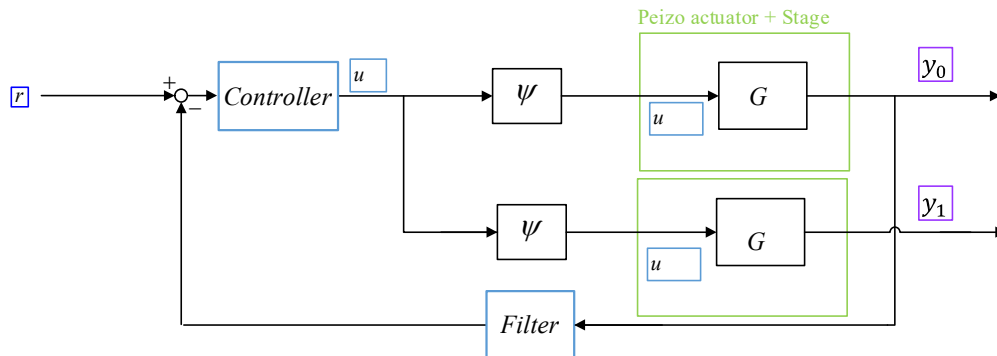
Fig. 6-2 Block diagram where the inner loop control eliminates the hysteresis

42

6.1.1　Measurement-based Hysteresis Observer

To measure the voltage consumption caused by hysteresis phenomenon precisely, the voltage after compensation which also actually derived to transducer and the voltage of operation voltage is needed. Typically, the actually applied voltage is estimated by the convolution of output and the inverse model of the system, and because the system is non-minimal phase system, it's even more burdensome. However, with the capacitor-connected structure, both minimal phase and non-minimal phase system u_p could be obtained

From equation 3-6, the effective voltage applied to the transducer u_p which is the remained voltage after hysteresis consumption, can be calculated with the estimated transformation ratio T_{em} by the equation

$$u_p = \frac{\left(C_e V_e - \Delta_p T_{em}\right)}{c_p} \tag{6.1}$$

So the estimation law of u_{remain} can be written as

$$u_{remain} = u_p + V_e = \frac{c_e V_e - T_{em} y}{c_p} + V_e \tag{6.2}$$
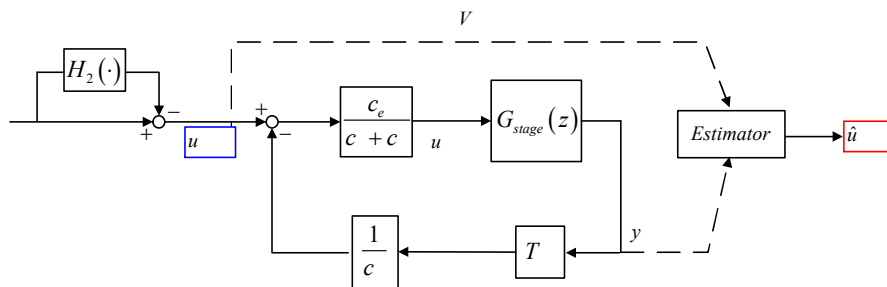
Fig. 6-3 General structure of u_{remain} estimator

In order to linearize the hysteresis, a voltage u_{cmp}, which is the estimation of the nonlinearity of hysteresis consumption u_h is added. The method of this compensator will be introduced following section. The corresponding equation of input voltage u is written as

$$u = u_{ctrl} + u_{cmp} \qquad (6.3)$$

Where u_{ctrl} is the desired operating voltage given by the outer-loop controller. Substitute (8.1) into Equation (8.2)

$$u_{remain} = u_{ctrl} + u_{cmp} - u_h \qquad (6.4)$$

Normally u_{cmp} is added to eliminate u_h. However, in this novel method, u_{cmp} is used to linearize the relationship between u_{ctrl} and u_{remain}. If compensator voltage u_{cmp} is calculated accurately, the previous equation becomes

$$u_{remail} = \psi \times u_{ctrl} \qquad (8.3)$$
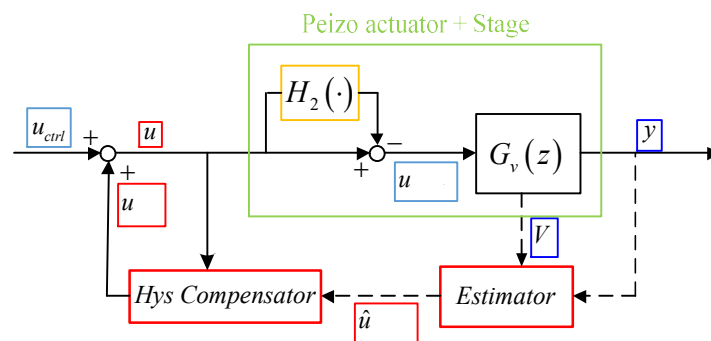
Fig. 6-4 Compensation principle of inner loop compensator

44
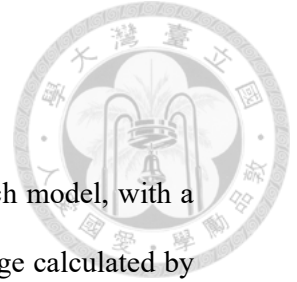
6.1.2 Measurement-based Hysteresis compensator

The hysteresis linearization method is based on a modified Preisach model, with a low-pass filter and a gain multiplier added after the compensation voltage calculated by the model. The structure of this method is shown in Fig. 6-5.
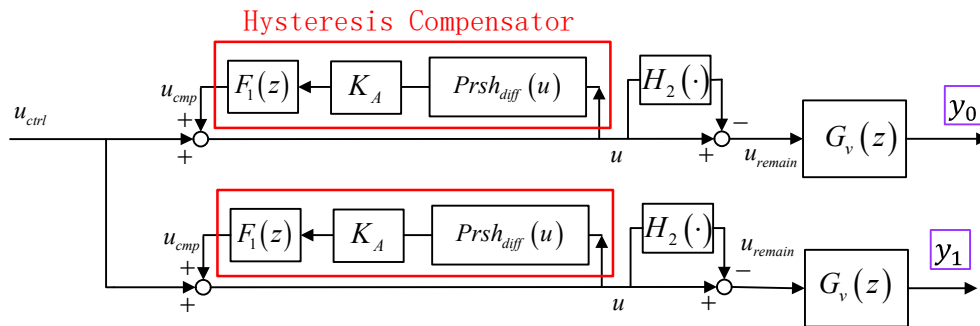
Fig. 6-5 Overall hysteresis compensator control structure

$Prsh_{diff}(\cdot)$ is the hysteresis-difference model, which calculate the difference of hysteresis between two consecutive inputs. Based on the rate-independent hysteresis model $Prsh(\cdot)$, $Prsh_{diff}(\cdot)$ is defined as

$$Prsh_{diff}(u) = Prsh(u) - Prsh(uz^{-1}) \tag{8.4}$$

The hysteresis-difference model is used to linearize the hysteresis phenomenon. According to the classical Preisach model compensation method, the compensation error caused by model-mismatch is mainly owing to the variation of the integrating area ΔS^+. Once the variation of the integrating area is compensated, the linearization of the hysteresis phenomenon is achieved, With the knowledge of the hysteresis phenomena introduced in chapter 4, the hysteresis phenomenon changes while either the frequency or the velocity of the input signal changes. It is reasonable to infer that the hysteresis differences under different frequencies can be described by one static hysteresis model

45

`

by amplifying certain amplitude K_A. The hysteresis difference between the consecutive

signals under another frequency ($f2$) could be obtained.

$$Prsh_{diff(f2)}(u) = K_A \times Prsh_{diff(s)}(u) \tag{6.7}$$

In order to compensate different signal without building rate-independent Preisach

model for each input signal, a changeable gain multiplier K_A is added. It is shown in Fig.

3-1 , the K_A is used to compensate different signal, which will greatly influence the

hysteresis linearization result. The amplitude of gain multiplier K_A will also affect the

tracking error, The better the compensator is, the less tracking error would be. The low

pass filter $F_1(z)$ is added to reduce the signal noise produced by the outer-loop controller

thus the compensation voltage will be less contaminated. The structure and function of

this filter is identical to the IIR filter introduced in 6.3.2.

6.2   Synchronized control

6.2.1   Synchronized control approaches

Basically there are three kinds of control structures in synchronized control

commonly used now by R.D.Lorenz [17] and Y.Koren [18].First one is Master-command

Approach as shown in Fig. 6-6. This structure is applying the total same moving

command to all axes. In this structure, two axes can be designed independently but usually

used in the condition of two axes are highly identical. Because the lack of communication

between two axes, when a sudden disturbance come in, the error will accumulate or even

worse, if two axes actuators have been coupled in hardware, this structure may leads to a

damage to stage.
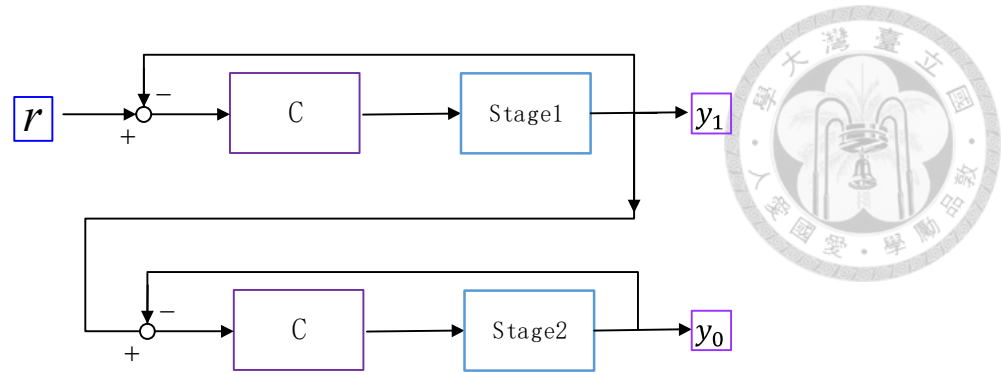
Fig. 6-6 Master-command Approach

And then, next one is Master-slave Approach as shown in Fig. 6-7. This structure need to select one axis as master axis and the other one which have a fast response as slave axis, put the output of master axis as the input of slave axis , make the slave to track the master axis' movement trajectory. The feature is that the independence of two axes control design is guaranteed, the difference of performances of two actuators is acceptable. However, the slave axis have the problem of time delay which may make the error accumulate as well and this structure also performs bad in higher frequency domain.
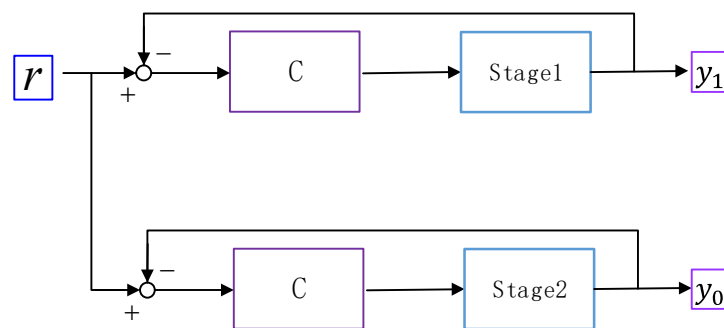
Fig. 6-7 Master-slave Approach

Finally, the Cross-coupled approach is proposed. This structure shown in Fig. 6-8 placed a unit called Synchronized error compensator. This unit can be seen as a communication between two axes, provides the function of synchronized control. The difficulty of this approach is the compensator's design method needs to be carefully

47

`

designed specifically referring to system characters.
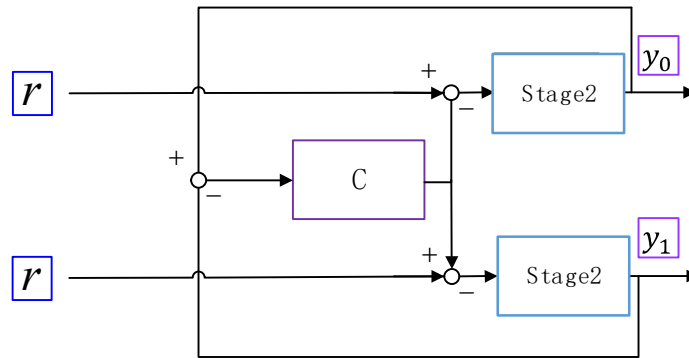
Fig. 6-8 Cross-coupled Approach

6.2.2 Synchronized control method

The Synchronized control in this paper is a combination of master command approach and a cross-coupled approach.

Except for this unit, other control methods of this plant works well. What's more, the two axes' control method is totally same .So, although the two axes have been coupling with each other, we can still apply master command approach to get a fast response not worrying about damaging the stage. In this paper, the command that simultaneously applied to two axes is the output of outer loop tracking controller that will be introduced next session.

As the cons mentioned, the performance of master command approach is not good enough, so cross-coupled approach is added to improve it. The method of design is shown below.

`
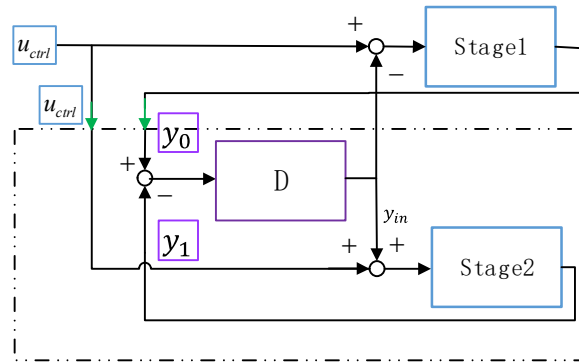
Fig. 6-9 Design method of synchronization

As you can see in Fig. 6-9. , the signal sources of stage2 are two: y_0 and u_{ctrl}. u_{ctrl} comes from master command approach as discussed. So if view y_0 as an input independently, it can be shown as Fig. 6-10
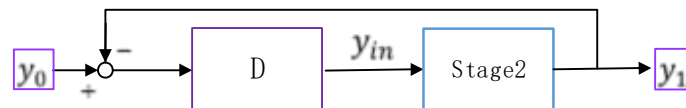
Fig. 6-10 Design method of signal y_0

The differences between two axes is thought as input which can be seen as a one axis input signal minus feedback. In another word, the goal of this unit is to make the output track the input low frequencies signal which is very similar to Master-slave approach. a plain PI controller is implemented in this unit. The P controller multiplies the current error by a weighting K_P. While I controller multiplies the accumulated error by a weighting K_I. The P controller is capable of reducing the error over all frequencies consistently, as the I controller features good tracking performance in low frequencies. The PI controller used in this thesis ensures a satisfying low-frequency performance and a adequate high-frequency control result. Equation (6.1) shows the transfer function of a discrete PI controller.

49

$$D(z) = K_p + K_i \frac{1}{1-z^{-1}} \qquad (6.8)$$

In a summary, the Synchronized control method include two parts: master command and cross-coupled approaches. The cross-coupled unit is designed with Master-slave approach's method, so the final synchronized controller is designed with the pros of both two methods but in a good balance.

6.3 Outer Loop Tracking Controller

There are two parts in the outer loop controller: the tracking controller $C(z)$ and a feedback filter $F(z)$. When designing the outer loop tracking controller, it is supposed that the ideal linearization is achieved. The system structure becomes like what is shown in Fig. 6-11.
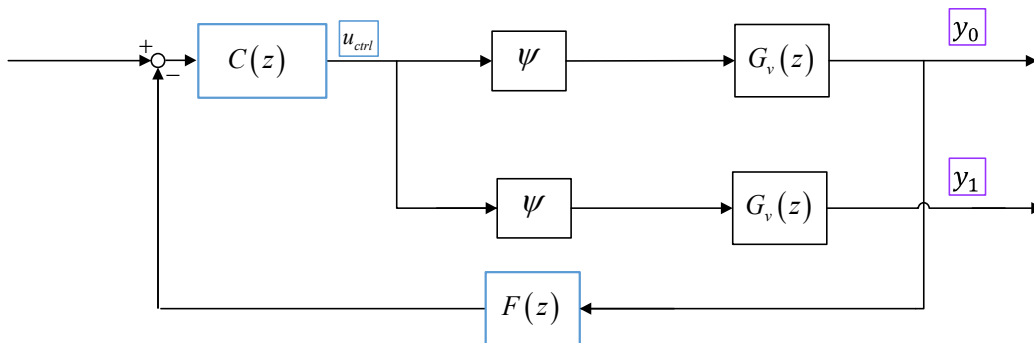
Fig. 6-11 Outer loop tracking control structure

6.3.1 Tracking Controller

In order to show the capability of the compensation method, another plain PI controller is implemented in tracking controller as well. As introduced before, PI controller can not only reduce the error but also provide good tracking performance in low frequencies input signals.

50

`

6.3.2　Feedback Filter

A first-order infinite impulse response filter (IIR filter) is chosen to diminish the high-frequency noise produced by the laser interferometer system and the environment. The IIR filter is implemented in the feedback path of the closed loop system. The transfer function of the IIR filter is shown below.

$$F(z) = \frac{1-\beta}{1-\beta z^{-1}} \tag{6.9}$$

where

$$0 \le \beta < 1 \tag{6.10}$$

The pole of $F(z)$ is a real pole at $z = \beta$. In order to obtain the corner frequency of $F(z)$, the conversion between Z-domain and S-domain is introduced as following

$$z = e^{sT_s} \tag{6.11}$$

Accordingly, the pole of the IIR filter in S-domain is

$$\frac{\ln(\beta)}{T_s} \tag{6.12}$$

In addition, as $z=1$ (when $s=0$), the static gain of $F(z)$ is equal to 1. As a result, the designed IIR filter is a low pass filter with corner frequency at $\ln(\beta^{-1})/(2\pi T_s)$ Hz.

The outer loop tracking controller is designed assuming the hysteresis phenomenon is linearized by the hysteresis compensator which is in the inner loop.

6.4　Stability Analysis

In best circumstances of hysteresis linearization of dual axes, the hysteresis phenomenon can be totally linearized and the relationship between u and u_{remain}

51

`

becomes $u_{remail} = \psi \times u_{ctrl}$ in both axes as well. However, the nonlinearity of the hysteresis might not be fully linearized in the real case. The non-linearized parts after hysteresis linearization can be regarded as uncertainty Δ_1 weighted with W_1 and Δ_2 with W_2. The relationship between u and u_{remain} is then changed to $u_{remain0} = (\psi + W_0\Delta_0) \times u$ as well as $u_{remain1} = (\psi + W_1\Delta_1) \times u$. The system structure is illustrated as Fig. 6-12 shows.
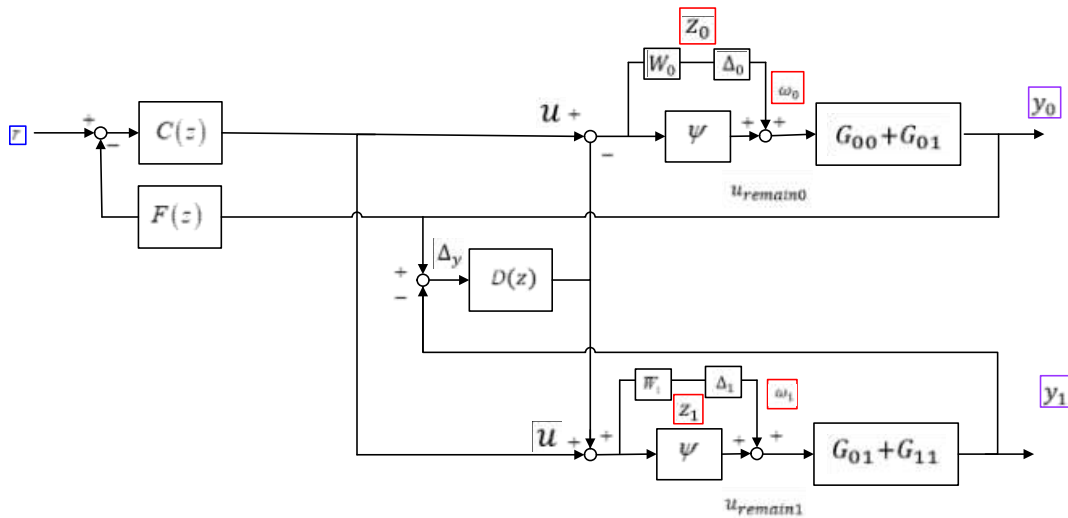
Fig. 6-12 Overall control structure with the equivalent weighted uncertainty and the small gain theorem

The best case and the worst case in this hysteresis consumption is no consumption and fully consumption, so all circumstances lie in range bounded two extreme situation which is $W_0\Delta_0 = 0$ /$W_1\Delta_1 = 0$ for perfect consumption and $W_0\Delta_0 = -\Psi$/$W_1\Delta_1 = -\Psi$ for a very poor consumption. From the experiment before, ψ can be found to be 0.66. The uncertainty weight W_1 and W_0 is bounded between [-0.66, 0.66] since the hysteresis is symmetric, where $-1 \le \Delta_0 \le 1$, $-1 \le \Delta_1 \le 1$.

52

`

For dual axes situation, from the relationships structure scheme shows, the equations are listed as
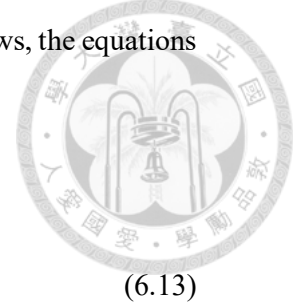
$$\begin{cases} z_0 = (u - D\Delta_y) \ W_0 \\ z_1 = (u + D\Delta_y) \ W_1 \\ \quad u = C(r - \ Fy_0) \\ \quad \Delta_y = y_0 - y_1 \\ y_0 = (\omega_0 + \Psi u \ )(G_{00} + G_{10}) \\ y_1 = (\omega_1 + \Psi u \ )(G_{01} + G_{11}) \end{cases} \qquad (6.13)$$

It can be derived that with $z_1/ \ z_2$ as outputs, while ω_0/ω_1 are inputs, this is MIMO system. The transfer matrix is

$$\begin{bmatrix} z_1 \\ z_2 \end{bmatrix} = \begin{bmatrix} m_{00} & m_{01} \\ m_{10} & m_{11} \end{bmatrix} \begin{bmatrix} \omega_0 \\ \omega_1 \end{bmatrix} \qquad (6.14)$$

where

$$m_{00} = (-D(G_{00} + G_{10}) - \frac{C(G_{00} + G_{10})(((G_{01} + G_{11}) - (G_{00} + G_{10}))\Psi D + 1)}{1 + C(G_{00} + G_{10})\Psi})W_0$$

$$m_{01} = (D(G_{01} + G_{11}) - \frac{C(G_{00} + G_{10})(((G_{01} + G_{11}) - (G_{00} + G_{10}))\Psi D + 1)}{1 + C(G_{00} + G_{10})\Psi})W_1$$

$$m_{01} = (D(G_{00} + G_{10}) - \frac{C(G_{00} + G_{10})(((G_{00} + G_{10}) - (G_{01} + G_{11}))\Psi D + 1)}{1 + C(G_{00} + G_{10})\Psi})W_0$$

$$m_{11} = (-D(G_{01} + G_{11}) - \frac{C(G_{00} + G_{10})(((G_{00} + G_{10}) - (G_{01} + G_{11})\Psi D) + 1)}{1 + C(G_{00} + G_{10})\Psi})W_1$$

From the designed controller, filter and system identification, $C(z) = 0.9 + 0.215\frac{1}{1-z^{-1}}$,

$F(z) = \frac{1-0.8}{1-0.8z^{-1}}$, $\psi = 0.66$, $G_{00}, G_{01}, G_{10}, G_{11}$ have been identified from Equation

(5.20), (5.21), (5.22) and (5.23).

As the result, by Small Gain Theorem, the stability criteria can be established as illustrated by the Robust Control Toolbox MATLAB[41]. The stable condition is then confirmed.

53

$$\| \begin{bmatrix} m_{00} & m_{01} \\ m_{10} & m_{11} \end{bmatrix} \|_\infty = 0.847 < 1 \tag{6.15}$$

Chapter 7   Experimental Validity
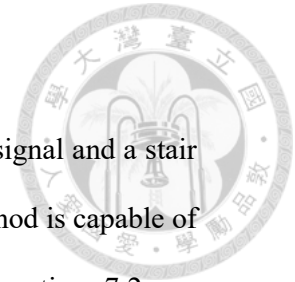
Series of experiments operated with 30Hz, 60Hz, 100Hz sinusoid signal and a stair signal are chosen for the experiment in order to justify the proposed method is capable of dealing signals with different frequencies. The control results in section 7.2 are experiments operated without hysteresis compensation, which are used to compare with the experiments done using hysteresis compensation in section 7.3.

7.1   Hysteresis Linearization

By using the method proposed in section 6.3, the nonlinearity of the hysteresis phenomenon between u_{ctrl} and u_{remain} could be reduced by adjusting K_A and the corner frequency of the filter $F_1(z)$. The experiments are done in open loop control under different frequencies to show that the hysteresis compensator is able to linearize the hysteresis. The results that the relationship between u_{remail} and u_{ctrl} can be described as $u_{remail} = \psi \times u_{ctrl}$ after linearization, where ψ =0.66. The amplified gain K_A and the β value of the filter $F_1(z)$ (which determines the corner frequency) chosen for each frequency are different.

(a)   (b)
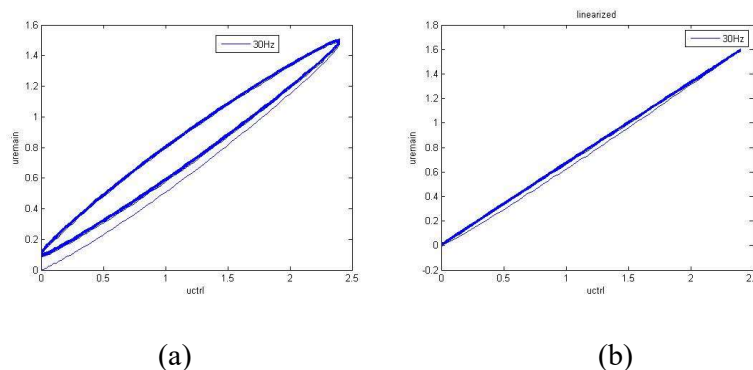
Fig. 7-1 (a)30Hz sine wave before linearized (b) after linearized

55

`
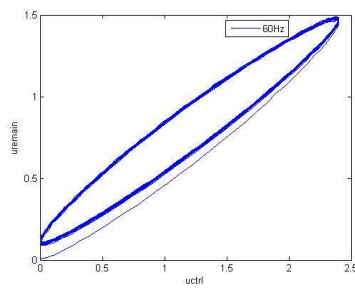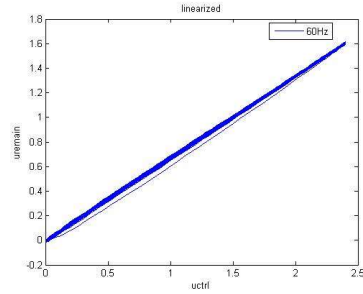
(a)   (b)

Fig. 7-2 (a)60Hz sine wave before linearized (b) after linearized
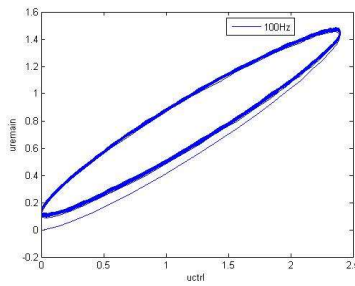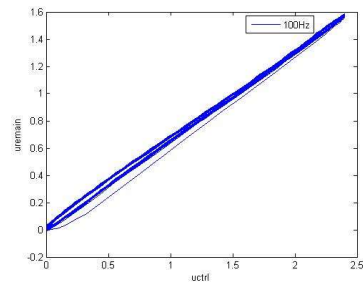
(a)   (b)

Fig. 7-3 (a)100Hz sine wave before linearized (b) after linearized

It is shown from the figures above that with the hysteresis linearization method, the relationship between u_{remail} and u_{ctrl} can be "squeezed" from an olive shape to nearly a line, which means the nonlinear phenomenon is reduced by the hysteresis compensator. In other words, the hysteresis phenomenon is "linearized". It is also shown that the higher the input frequency is, the poorer the hysteresis linearization works. Since the hysteresis phenomenon changes differently under high frequency, the approximation of hysteresis difference may not be able to reach perfectly. Due to Synchronized control, the operating voltages on dual axis piezo actuators are different, so the specific parameters are designed to finish compensator. Following Table 7-1 shows the specific parameters selected after experiments. The K_{A0} means the compensator on the axis 0, K_{A1} on the axis 1 as the same, and the parameter of filter are shared together.

56

	30Hz	60Hz	100Hz
β of $F_1(z)$	0.963	0.9518	0.8
K_{A0}	13.6	8.5	6.1
K_{A1}	13.5	8.3	5.8

Table 7-1 β value and K_{A0}, K_{A1} under different frequencies

7.2 Without Synchronized control

In this and next sections, experiments are done without synchronized unit and with it as a comparison. Except for synchronized control part, all other control methods are the same including hysteresis linearization and outer loop control which consists of a plain PI tracking controller and a low pass filter that can be used to reduce the influence of high frequency disturbance are implemented for the system. The results are used to shown how synchronized control influence the two axes' displacements difference.
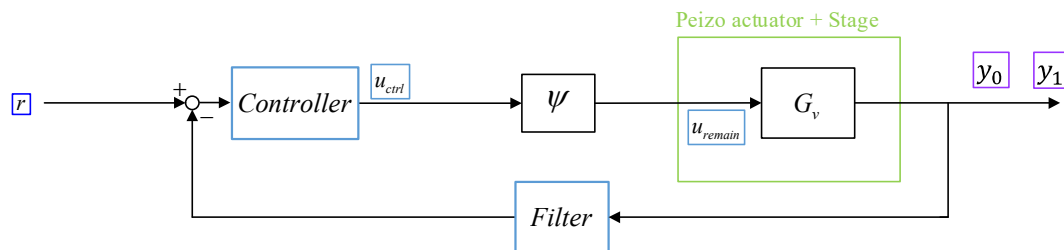
Fig. 7-4 Control structure without synchronized control

The parameters of PI controller in outer loop control are always fixed to $\left(K_p, K_i\right) = (0.9, 0.215)$. The β value, which influences the corner frequency of the filter $F(z)$ is fixed at the value of 0.8, which is corresponding to the corner frequency of 177.572Hz. Due to the lack of synchronized, the drive voltages on two axes are the same ,so the hysteresis linearization parameters are same in dual axes.

57

7.2.1　Without synchronization: Stair Signal
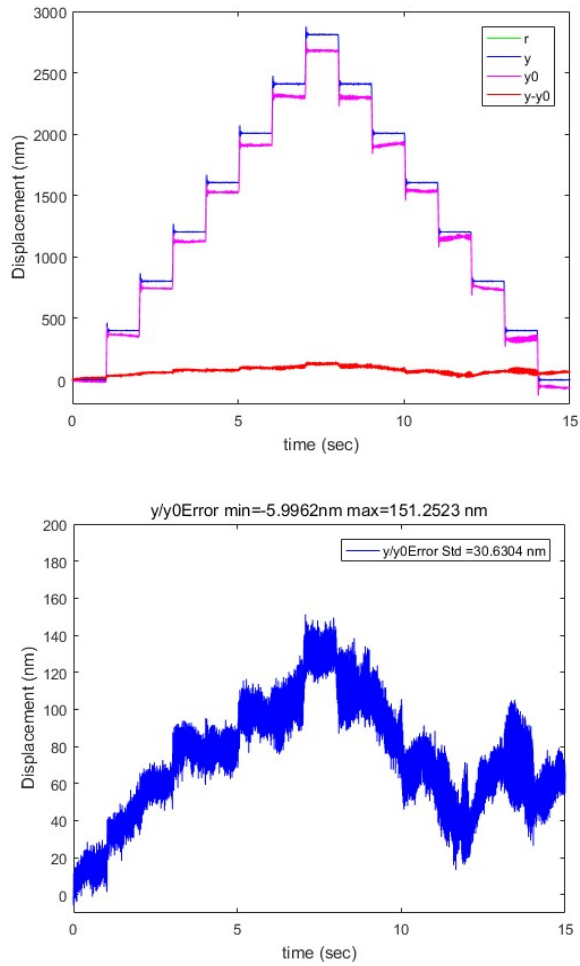
Fig. 7-5 Control results without synchronized control stair signal

Reference Signal	stair
Outer loop control	Yes
Synchronized control	No
Inner loop control	Yes
PI parameter $\left(K_p , K_i \right)$	(0.9 , 0.215)

`

β value of IIR filter $F(z)$	0.8(177Hz)
β value of IIR filter $F_1(z)$	0.963(30Hz)
K_A	13.6
Error Range	[-6.0 , 151.3] nm

Table 7-2 Control results without synchronized control stair signal

7.2.2 Without synchronization: 1.2sin(30Hz)

Fig. 7-6 Without synchronization 60Hz sine wave

Reference Signal	1.2+1.2sin(30Hz)

`

Outer loop control	Yes
Synchronized control	No
Inner loop control	Yes
PI parameter $\left(K_p, K_i\right)$	(0.9 , 0.215)
β value of IIR filter $F(z)$	0.8(177Hz)
β value of IIR filter $F_1(z)$	0.963(30Hz)
K_A	13.7
Error Std.	13.4 nm
Error Range	[-4.6 , 79.7] nm

Table 7-3 Control Results without synchronized control 30Hz sine wave

7.2.3　Without synchronization: 1.2sin(60Hz)
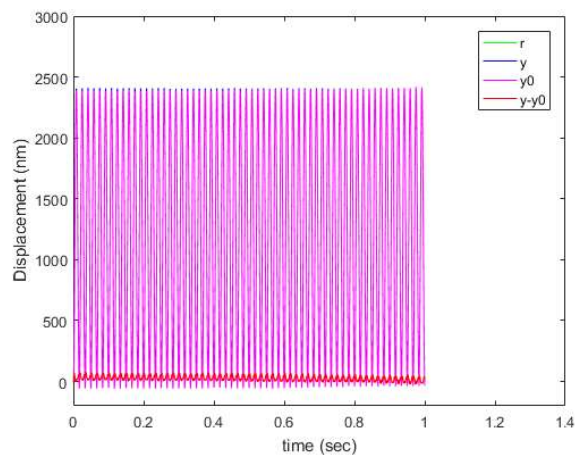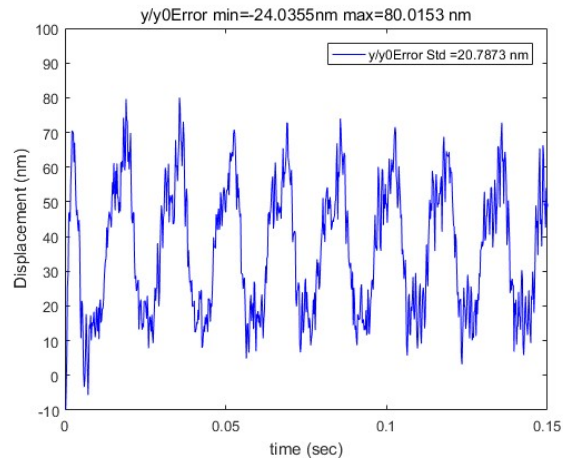
Fig. 7-7 Without synchronization 60Hz sine wave

Reference Signal	1.2+1.2sin(60Hz)
Outer loop control	Yes
Synchronized control	No
Inner loop control	Yes
PI parameter $\left(K_p , K_i \right)$	(0.9 , 0.215)
β value of IIR filter $F(z)$	0.8(177Hz)
β value of IIR filter $F_1(z)$	0.9158(60Hz)
K_A	8.5
Error Std.	20.8 nm
Error Range	[-24.0 ,80.0] nm

Table 7-4 Control Results without Synchronized control 60Hz sine wave

7.2.4 Without synchronization: 1.2sin(100Hz)
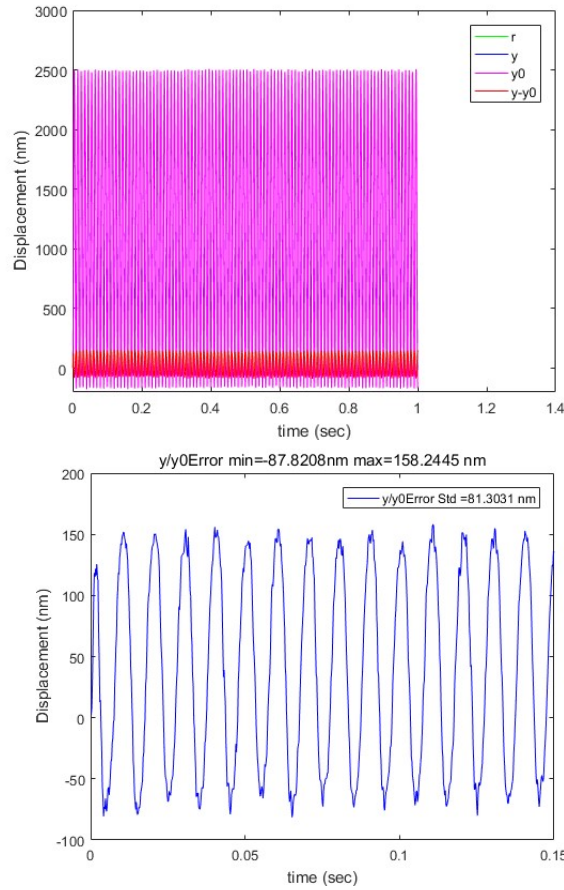
Fig. 7-8 Without synchrony 100Hz sine wave

Reference Signal	1.2+1.2sin(100Hz)
Outer loop control	Yes
Synchronized control	No
Inner loop control	Yes
PI parameter $\left(K_p , K_i \right)$	(0.9 , 0.215)
β value of IIR filter $F(z)$	0.8(177Hz)
β value of IIR filter $F_1(z)$	0.8(177Hz)
K_A	6.1

Error Std.	81.3 nm
Error Range	[-87.8 , 158.2 nm

Table 7-5 Control Results without Synchronized control 100Hz sine wave
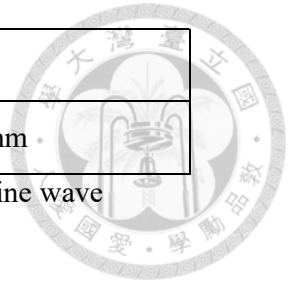
7.3 With Synchronized control

The parameters of PI controller in outer loop control are always fixed to $\left(K_p, K_i\right) = (0.9, 0.215)$. The β value, which influences the corner frequency of the filter $F(z)$ is fixed at the value of 0.8, which is corresponding to the corner frequency of 177.572Hz. When Synchronized control part is on, the parameters of PI controller in it is selected as $\left(D_p, D_i\right) = (0.2, 002)$

7.3.1 With synchronization: Stair Signal
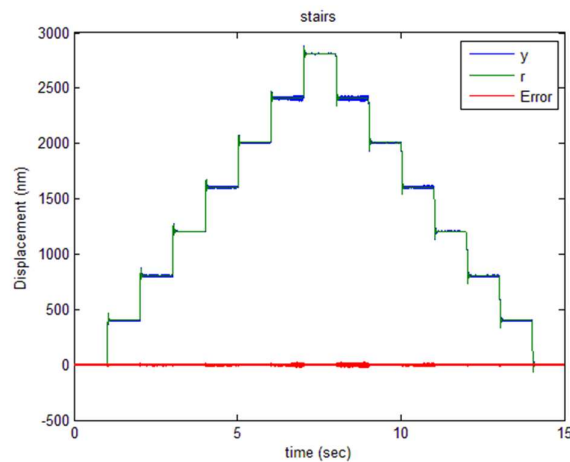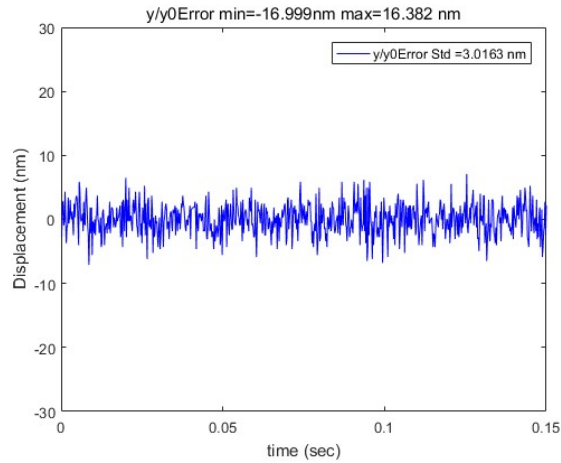
Fig. 7-9 Control Results with synchronization Stair Signal

Reference Signal	stair
Outer loop control	Yes
Synchronized control	Yes
Inner loop control	Yes
PI parameter $\left(K_p , K_i\right)$	(0.9 , 0.215)
Synchronized PI parameter $\left(D_p, D_i\right)$	(0.21 , 0.02)
β value of IIR filter $F(z)$	0.8(177Hz)
β value of IIR filter $F_1(z)$	0.963(30Hz)
K_{A0}	13.6
K_{A1}	13.6
Error Std.	3.0 nm
Error Range	[17.0 , 16.4] nm

Table 7-6 Control Results without synchronized control Stair Signal

`

7.3.2 With synchronization: 1.2sin(30Hz)
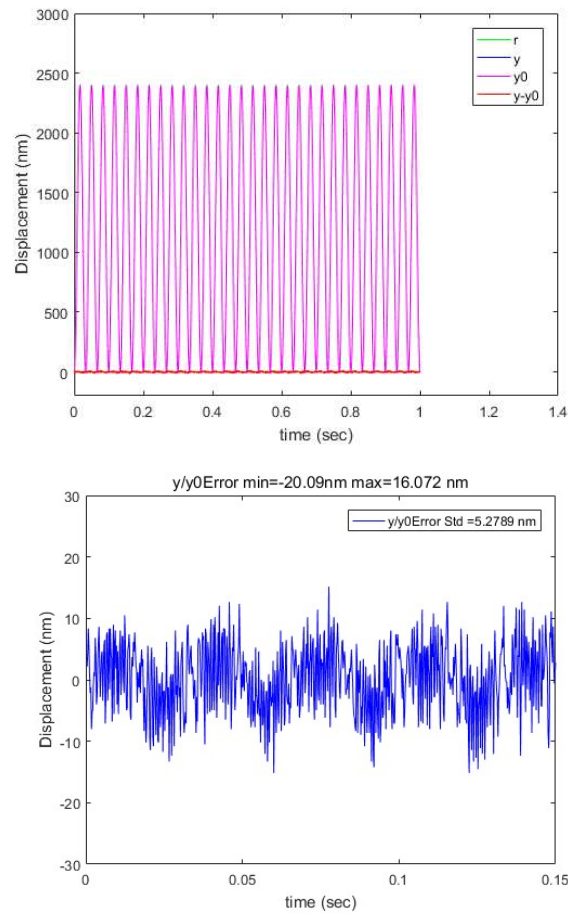
Fig. 7-10 With synchronization 60Hz sine wave

Reference Signal	1.2+1.2sin(30Hz)
Outer loop control	Yes
Synchronized control	Yes
Inner loop control	Yes
PI parameter $\left(K_p, K_i\right)$	(0.9 , 0.215)
Synchronized PI parameter $\left(D_p, D_i\right)$	(0.21 , 0.02)
β value of IIR filter $F(z)$	0.8(177Hz)
β value of IIR filter $F_1(z)$	0.963(30Hz)

`

K_{A0}	13.7
K_{A1}	13.7
Error Std.	5.3nm
Error Range	[-20.1 , 16.1] nm

Table 7-7 Control Results with synchronized control 30Hz sine wave

7.3.3 With synchronization: 1.2sin(60Hz)

Fig. 7-11 With synchronization 60Hz sine wave

Reference Signal	1.2+1.2sin(60Hz)

66

`

Outer loop control	Yes
Synchronized control	Yes
Inner loop control	Yes
PI parameter $\left(K_p , K_i \right)$	(0.9 , 0.215)
Synchronized PI parameter $\left(D_p, D_i \right)$	(0.21 , 0.02)
β value of IIR filter $F(z)$	0.8(177Hz)
β value of IIR filter $F_1(z)$	0.9158(60Hz)
K_{A0}	8.5
K_{A1}	8.3
Error Std.	7.4 nm
Error Range	[-24.1 ,25.3] nm

Table 7-8 Control Results with Synchronized control 60Hz sine wave

7.3.4 With synchronization: 1.2sin(100Hz)
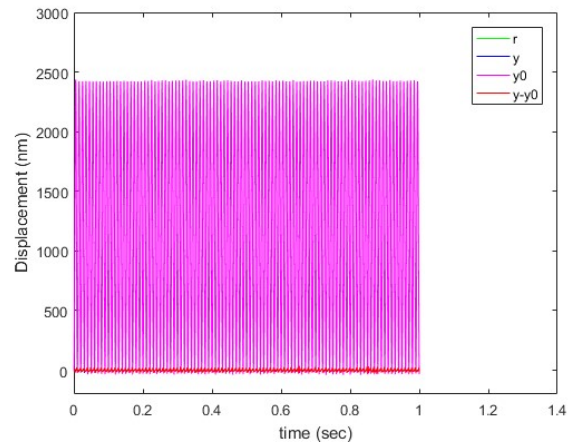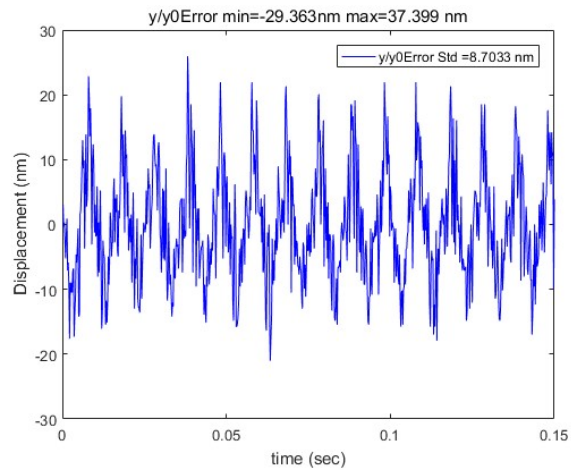
Fig. 7-12 with synchronization 100Hz sine wave

Reference Signal	1.2+1.2sin(100Hz)
Outer loop control	Yes
Synchronized control	Yes
Inner loop control	Yes
PI parameter $\left(K_p, K_i\right)$	(0.9 , 0.215)
Synchronized PI parameter $\left(D_p, D_i\right)$	(0.21 , 0.02)
β value of IIR filter $F(z)$	0.8(177Hz)
β value of IIR filter $F_1(z)$	0.8(177Hz)
K_{A0}	6.1
K_{A1}	5.8
Error Std.	8.7 nm
Error Range	[-29.4 , 37.4] nm

Table 7-9 Control Results with Synchronized control 100Hz sine wave

68

7.4   Control Performance

Due to Synchronized control unit increases the complexity of control method of the stage, the control performance in one axis is getting worse than without it. However, with proper design in parameters, the balance between synchronized control and axis displacement control performance can be found. Although synchronized control unit is added, the performance remains good.

The parameters of PI controller in outer loop control are always fixed to $\left(K_p, K_i\right) = (0.9, 0.215)$. The β value, which influences the corner frequency of the filter $F(z)$ is fixed at the value of 0.8, which is corresponding to the corner frequency of 177.572Hz. When Synchronized control part is on, the parameters of PI controller in it is selected as $\left(D_p, D_i\right) = (0.21, 002)$

7.4.1   Control result: Stair signal

69
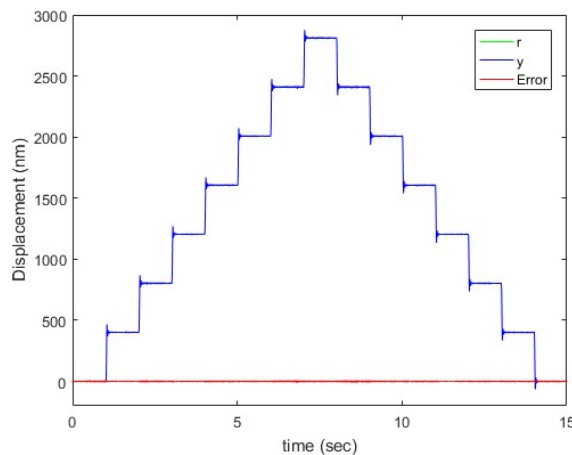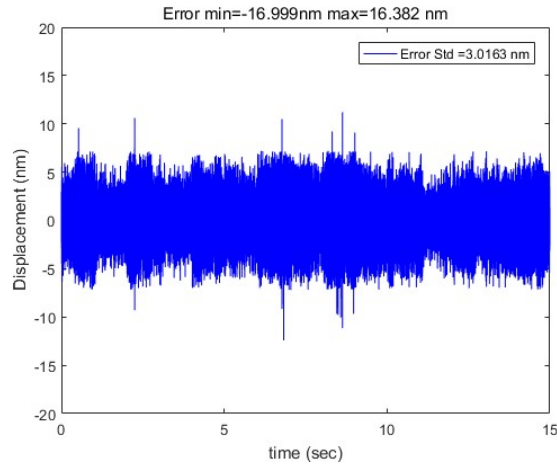
Fig. 7-13 Control result of stair signal synchronization linearization

Reference Signal	Stair Signal
PI parameter $\left(K_p , K_i\right)$	(0.9 , 0.215)
Synchronized PI parameter $\left(D_p, D_i\right)$	(0.21 , 0.02)
β value of IIR filter $F(z)$	0.8(177Hz)
β value of IIR filter $F_1(z)$	0.963(30Hz)
K_{A0}	13.6
K_{A1}	13.6
Error Std.	3.0 nm
Error Range	[-12.4 , 11.2] nm

Table 7-10 Control result and parameter setting of Stair Signal

7.4.2 Control result: 1.2sin(30Hz)
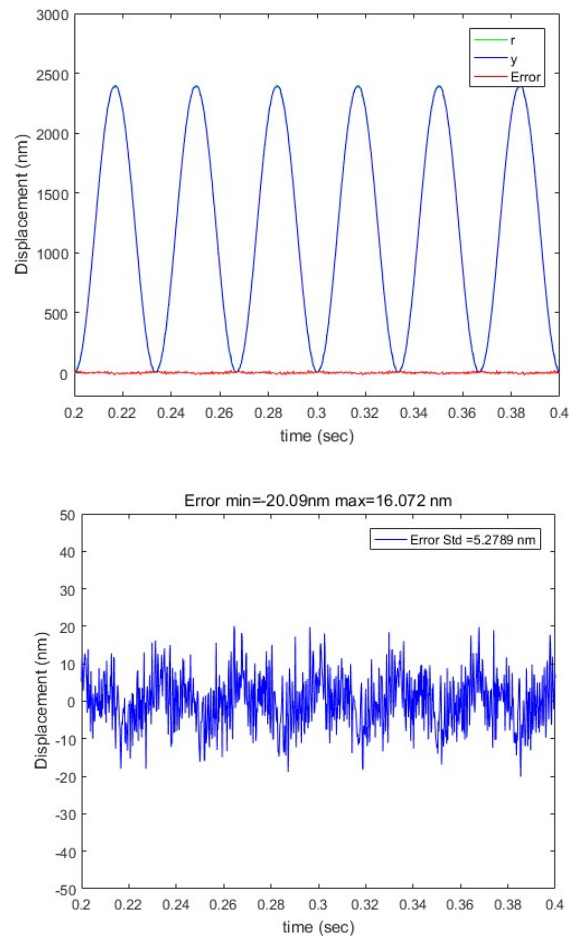
Fig. 7-14 Control result of 30Hz sine wave synchronization linearization

Reference Signal	1.2+1.2sin(30Hz)
Control parameter $\left(K_p , K_i \right)$	(0.9 , 0.215)
Synchronized PI parameter $\left(D_p, D_i \right)$	(0.21 , 0.02)
β value of IIR filter $F(z)$	0.8(177Hz)
β value of IIR filter $F_1(z)$	0.963(30Hz)
K_{A0}	13.7
K_{A1}	13.7

71

Error Std.	5 nm
Error Range	[-20.1 , 16.1] nm

Table 7-11 Control result and parameter setting of 30Hz sine wave
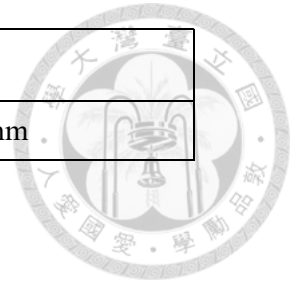
7.4.3 Control result: 1.2sin(60Hz)

Fig. 7-15 Control result of 60Hz sine wave synchronization linearization

Reference Signal	1.2+1.2sin(60Hz)
Control parameter $\left(K_p , K_i \right)$	(0.9 , 0.215)
Synchronized PI parameter $\left(D_p, D_i \right)$	(0.21 , 0.02)
β value of IIR filter $F(z)$	0.8(177Hz)

72

`

β value of IIR filter $F_1(z)$	0.9158(60Hz)
K_{A0}	8.5
K_{A1}	8.3
Error Std.	7.1 nm
Error Range	[-19.7 , 21.1] nm

Table 7-12 Control result and parameter setting of 60Hz sine wave
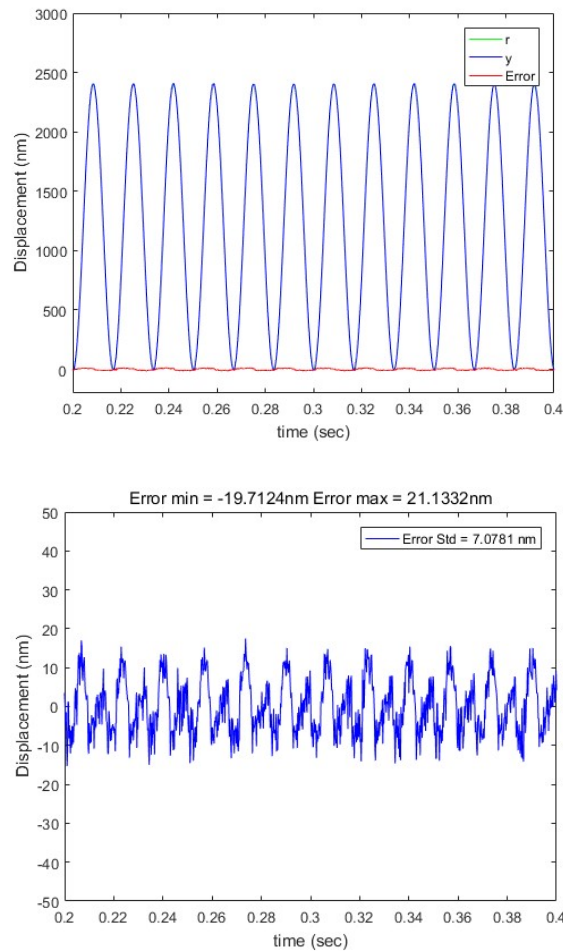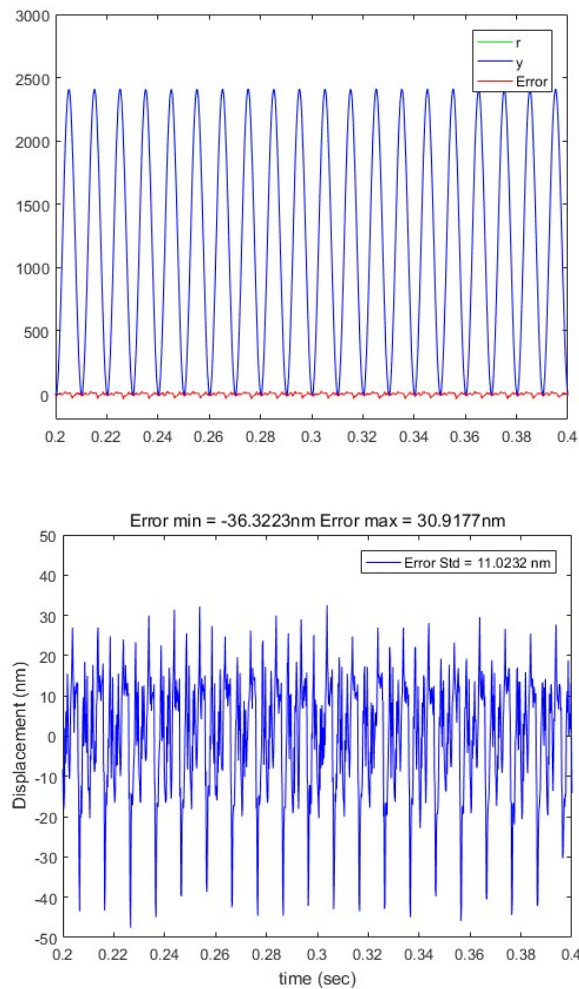
7.4.4   Control result: 1.2sin(100Hz)

Fig. 7-16 Control result of 100Hz sine wave synchronization linearization

Reference Signal	1.2+1.2sin(100Hz)

`

Control parameter $\left(K_p , K_i\right)$	(0.9 , 0.215)
Synchronized PI parameter $\left(D_p, D_i\right)$	(0.21 , 0.02)
β value of IIR filter $F(z)$	0.8(177Hz)
β value of IIR filter $F_1(z)$	0.8(177Hz)
K_{A0}	6.1
K_{A1}	5.8
Error Std.	11.2nm
Error Range	[-36.3, 30.9] nm

Table 7-13 Control result and parameter setting of 100Hz sine wave

7.5 Synchronized control methods Comparison

In this section, the Synchronized control methods produced in this thesis will be compared with some other methods proposed in the other paper. The Synchronized control of piezo-actuated stage haven't been researched, but the methods of other actuated stage may also works in this stage.

7.5.1 Comparing with Adaptive Fuzzy Control

Due to the high interpretability and simplicity, Fuzzy Control is used to form synchronous motor control system as WB.Shih *el at* [19]. What's more, it used control rules to describe the system' variables relationship which means the controller does not need to be formulated. As those features, this method is usually applied on nonlinear, time-varies, imperfection's Models. And it is easy-controlled, self-adaptive with good Robustness as well as Fault Tolerance so that can be used well in Hysteresis.

However, in this thesis, Hysteresis phenomenon has already been compensated up

74

`

by Hysteresis linearization. If Hysteresis linearization works well, the system is linear. Besides, fuzzy control rules are roughly control adjust which is not precise enough in this case because the outer and inner control loop have improved the control result a high standard. Last but not least, with varies kinds input signals, the response need to be really fast but fuzzy control performs bad in higher frequencies so it cannot meet up the requirements.

7.5.2 Comparing with Robust Cross-Coupled Control

Suppose ε_0 is the difference between master axis and slave axis, which is the error haven't cross coupled yet, after a cross-coupled controller, the output ε is the error after coupled. Cross-coupled unit is represented as D, stage's actuators are G_0 and G_1, compensator is thought as ideal with a symbol of F. The relationship of ε_0 and ε is as following:

$$\varepsilon = \frac{1}{1+D\left(\frac{G_{01}+G_{11}}{\left(1+F(G_{00}+G_{10})(1+\emptyset_0)\right)} - \frac{G_{00}+G_{10}}{\left(1+F(G_{01}+G_{11})(1+\emptyset_1)\right)}\right)} \varepsilon_0$$

$$(7.1)$$

From which, it could be easily to view a sophistical movement cross-coupled system as a standard SISO system as shown in Fig. 7-17
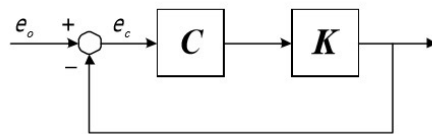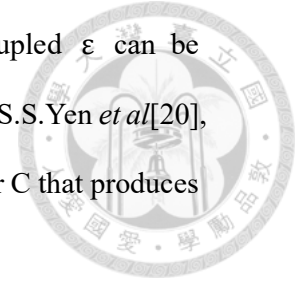

Fig. 7-17 Equivalent standard SISO system

In which C = D, K = $\dfrac{G_{01}+G_{11}}{\left(1+F(G_{00}+G_{10})(1+\emptyset_0)\right)} - \dfrac{G_{00}+G_{10}}{\left(1+F(G_{01}+G_{11})(1+\emptyset_1)\right)}$

`

So if the controller C is designed properly, the error after coupled ε can be

$$C(s) = \frac{1}{s}\hat{C}(s)$$ suppressed as Synchrony achieved. Based on S.S.Yen *et al*[20],

when following four design requirements are satisfied for a compensator C that produces

satisfactory stability.

(1)

(2) C(s) is the minimum phase rational function.

(3) The rational function CK(s) is strictly proper, and has no real zeros equal to or

larger than one.

(4) The rational function CK(s) has both positive gain and no real zeros equal to or

larger than one phase margins in frequency domain analysis

As proved, the stage in this case can use this design requirements as well as analyzed

before. While in experiments, the experiment shows a better tracking result in step input

than current one, but almost no effect in a higher frequency signal like 1.2+1.2*sin(30Hz).

From the view of tracking opinion introduced before, take simplest controller that

satisfied all four conditions C(s) = $\frac{1}{s}$. As shown in Fig. 6-10, it is equivalent to an I

controller (integrator) that cannot track sinusoidal wave.

7.6   Control result Comparison to other methods

In this section, the control results produced by control method proposed in this thesis

will be compared with some other methods proposed in the other papers.

7.6.1   Comparing with Disturbance Observer Based Hysteresis Observer

The disturbance observer (DOB) based hysteresis observer proposed by J. A. Yi et

al. [11] is a method which regard hysteresis as disturbance. An observer based on system

76

`

inversion is implemented to estimates the voltage lost. The DOB method is able to satisfy the performance requirement under high frequency operation. The Hysteresis linearization method proposed in this thesis will be used to compare with the control results of DOB based hysteresis observer. [11].
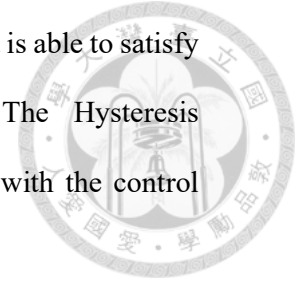
The amplitude of the input signals for comparing these two method is 0.5 micro-meter under 1Hz, 10Hz and 100Hz. The tracking error of the DOB based hysteresis observer is shown in Fig. 7-18 while the tracking error of method proposed in this thesis it is shown in Fig. 7-19. According to these two figures, with input under frequency of 1Hz, the tracking error of DOB based hysteresis observer is much higher while the tracking errors of two methods operated with signal under frequency of 10Hz and 100Hz are close.

Because the lack of necessary information of original data, the performance of synchroinzed control cannot be conpared. Following other papers exist same problem. However, by control bolck diagram , some briefly comparison are made logically. As this case, DOB based hysteresis observer method are applied on the staged driven only by one actuator

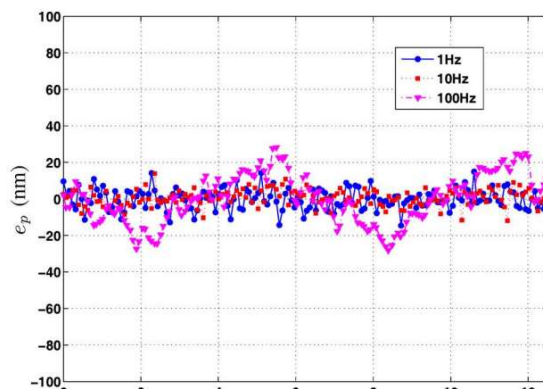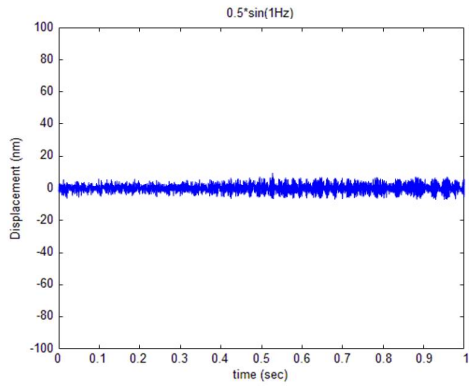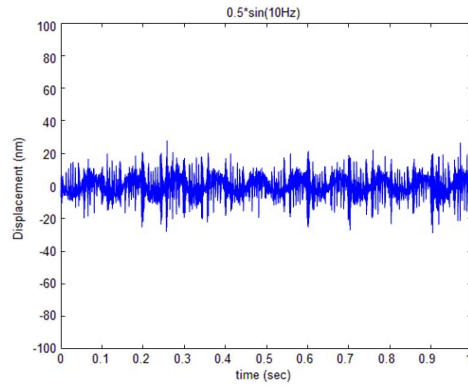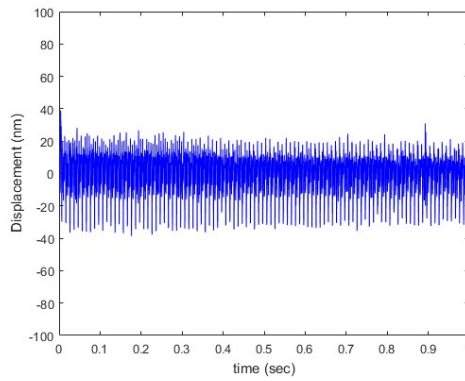Fig. 7-18 Tracking error of DOB based hysteresis observer. (The reference signal are

1Hz, 10Hz and 100Hz sine wave with amplitude of 0.5 micro-meter.) [11]

77

(a)

(b)

(c)

Fig. 7-19 Tracking error of Hysteresis compensation method. (a) 1Hz. (b) 10Hz. (c)
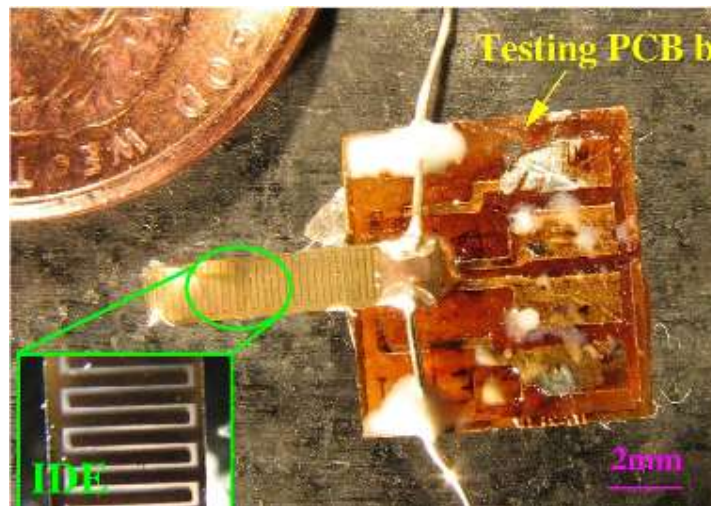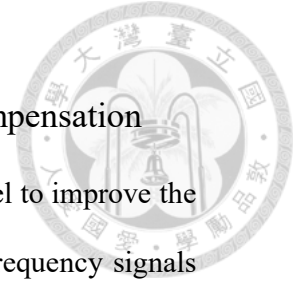
100Hz (Sine wave with amplitude of 0.5 micro-meter)

Fig. 7-20 Mechanical contracture of DOB based hysteresis observer method[11].

78

`

7.6.2   Comparing with Direct Inverse Hysteresis Model Compensation

The direct approach of deriving the inverse Prandtl-Ishlinskii model to improve the tracking performance proposed by Qin et al[3]. is limited under low frequency signals since there will be inevitable modeling error at fast trajectories. On the other hand, the hysteresis linearization is capable of reducing the hysteresis nonlinearity for signals under high frequencies. Thus the outer loop tracking controller is able to maintain the accuracy of high frequency tracking performance. The proposed method in this thesis provides better tracking performance for both slow and fast trajectory than the direct inverse hysteresis model compensation.

Despite both high frequencies and low frequencies are tries in input signal, with the highest frequency proposed by Qin et al[3] much more smeller than 100hz which has been proved effective by the synchronized unit used in this thesis, With that improvement in synchronization , the control method proposed should perform better.
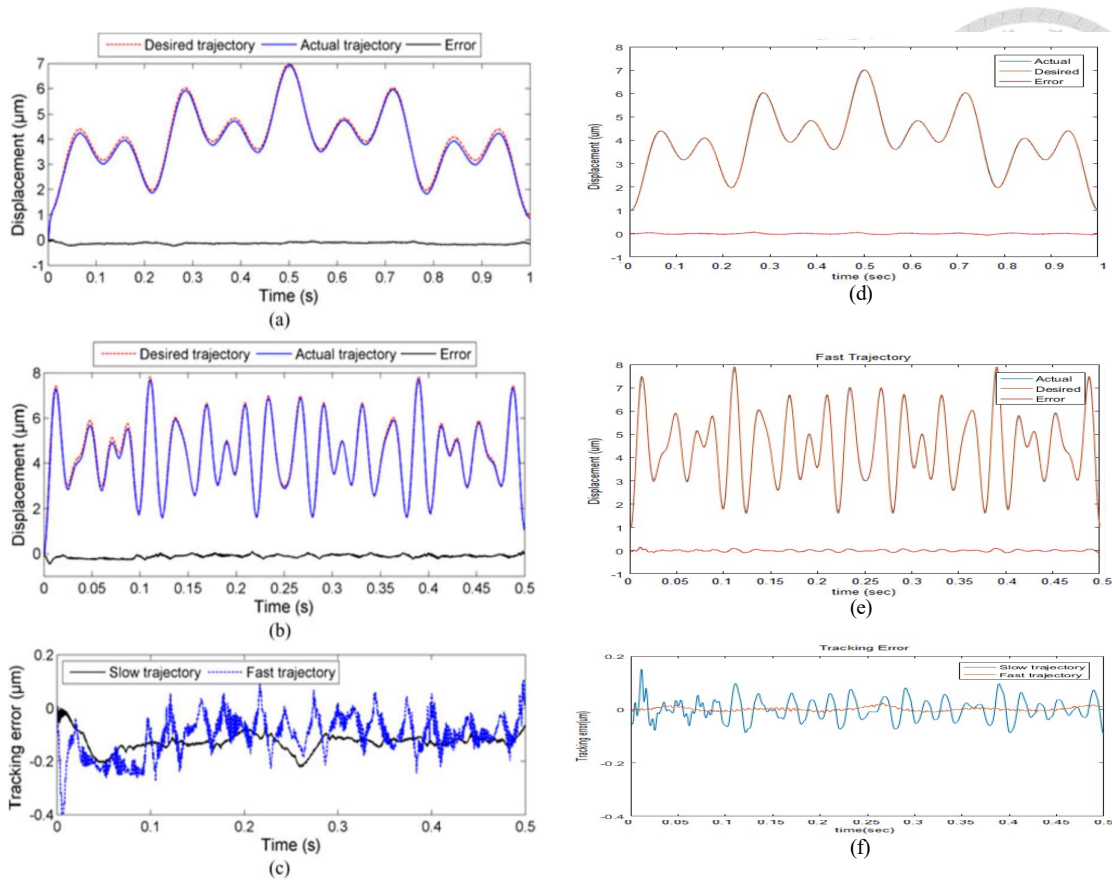
Fig. 7-21 Comparison of the trajectory tracking result. (a), (b) and (c) are from Qin et al.

(a) Slow trajectory from (b) Fast trajectory (c) Tracking errors. (d), (e) and (f) are from

this thesis. (d) Slow trajectory (e) Fast trajectory (f) Tracking errors

7.6.3   Comparing with Charge Feedback Control

L. S. Chen et al. [16] proposed a control method which uses the voltage drop on the external capacitance as the feedback signal while the control method in this thesis only uses the voltage drop to identify the hysteresis phenomenon. The measured voltage signal is used to calculate the Presiach model only. Four different reference signals (Stair signal, sine waves with frequencies under 30Hz, 60Hz, 100Hz of which the amplitude is 1.2 micro-meter respectively) are chosen to compare the tracking performance of these two methods.

80
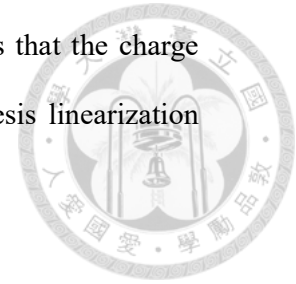
The control results of stair signal are shown below, which shows that the charge feedback control is suffer from the drift phenomenon, but the hysteresis linearization method is not.

(a)   (b)
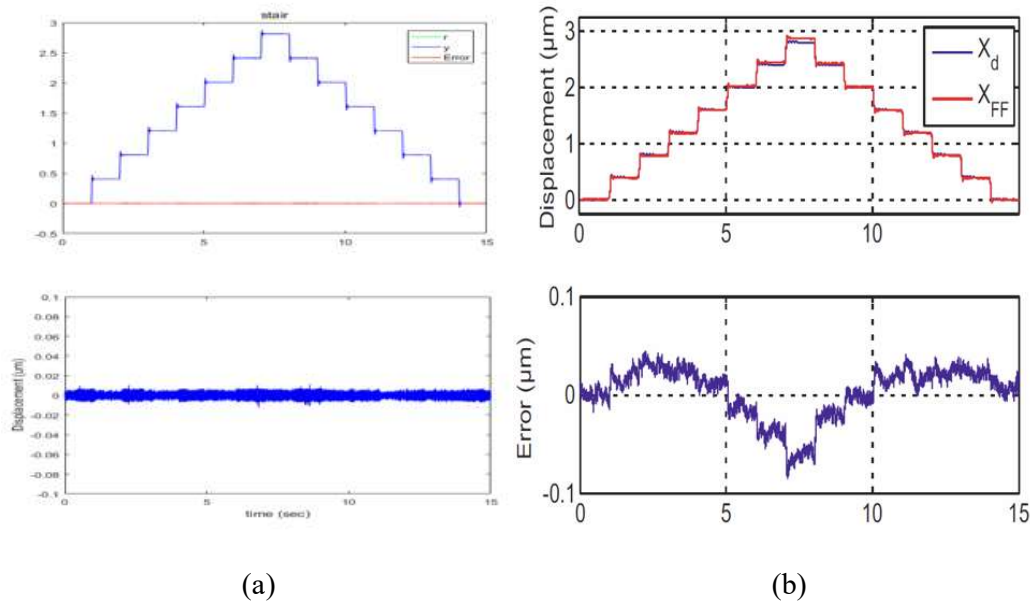
Fig. 7-22 Control results of stair signal: (a) Synchronization and Linearization, (b) Charge feedback control.

The tables below shows the overall control results of the experiments done with different signals. It is shown that the tracking control result of Synchronization and Linearization method is much better than Charge Control.

Due to the data of dual axes movements are not taken in that method, the variable representing synchronization situation cannot be calculated as well. However, considering there's no any control method applied on this stage, the performance of synchronization attribute is thought as poor which might be similar to section 7.2.

	Stair signal	30Hz	60Hz	100Hz
Charge Control	Drift	19.5	25	96

81

	Stair Signal	30Hz	60Hz	100Hz
Synchronization & Linearization	3.0	5	7.1	11.2

Fig. 7-23 Standard deviation of the tracking error comparison with Charge Control.

(unit: nm)

	Stair Signal	30Hz	60Hz	100Hz
Charge Control	[-80 , 50]	[-40 , 83]	[-89 , 130]	[-695 , 396]
Synchronization & Linearization	[-12.4 , 11.2]	[-20.1 ,16.1]	[-19.7, 21.1]	[-36.3 , 30.9]

Fig. 7-24 Error range comparison with Charge Control (unit: nm)

7.6.4 Comparing with Hybrid Hysteresis Compensation of Hysteresis Observer and Preisach Model Estimator

S. T. Liu et al. [35] proposed that using measurement-based hysteresis observer, with voltage feedback, the hysteresis phenomenon can be reduced and eliminated by the tracking controller, while in this thesis, the compensation method is clearer and the control result is better. Four different reference signals (Stair signal, sine waves with frequencies under 30Hz, 60Hz, 100Hz of which the amplitude is 1.2 micro-meter respectively) are chosen to compare the tracking performance of these two methods.

Obstacles of comparing the results of dual axes error still exists in this method. So the way of handling it is the same as it was. When Observe the control block and measurement system in this method, there is no any synchronization control is involved as well as measurement units. From this aspect, the result is regarded as poor.
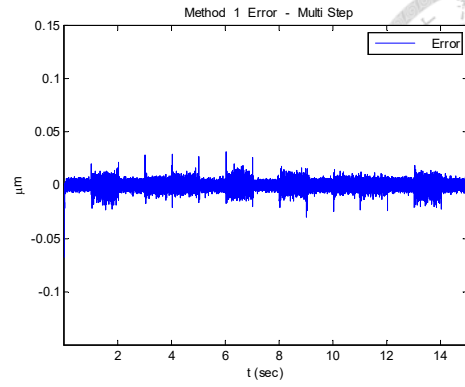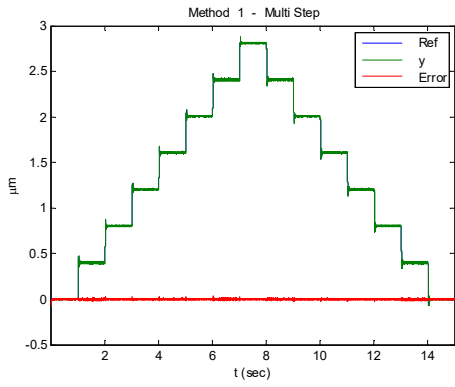
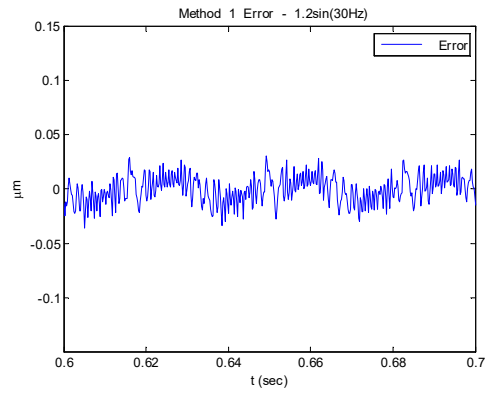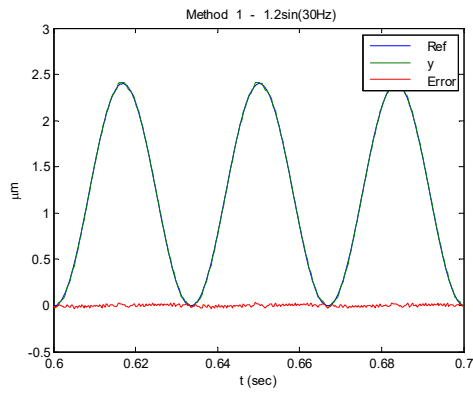Fig. 7-25 Control result of stair signal from Liu

Fig. 7-26 Control result of 30Hz sine wave from Liu
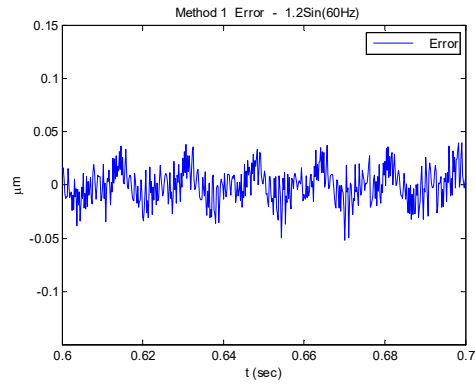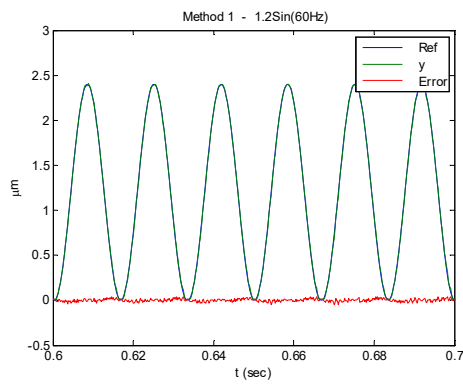
Fig. 7-27 Control result of 60Hz sine from Liu

83
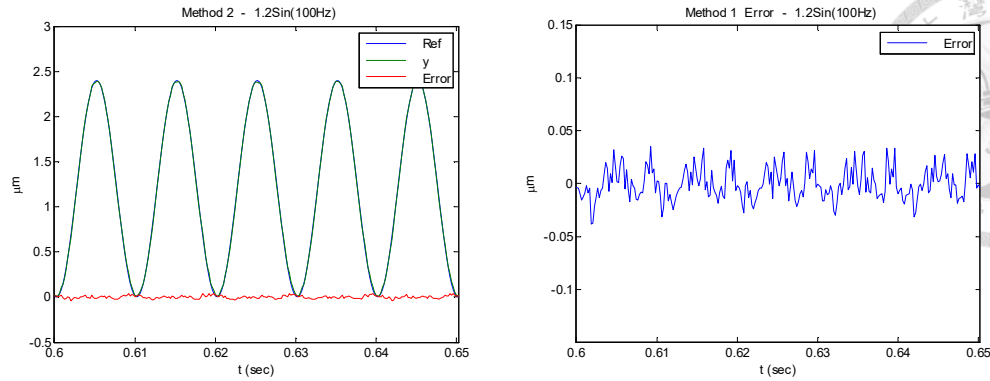
Fig. 7-28 Control result of 100Hz sine from Liu

	Stair	30Hz	60Hz	100Hz
Liu	3.4	12.5	16.2	15.4
Synchronization & Linearization	3.0	5	7.1	11.2

Fig. 7-29 Standard deviation of the tracking error comparison with Liu(unit: nm)

	Stair	30Hz	60Hz	100Hz
Liu	[-15 , 15]	[-30 , 30]	[-37, 37]	[-35 , 35]
Synchronization & Linearization	[-12.4 , 11.2]	[-20.1 ,16.1]	[-19.7, 21.1]	[-36.3 , 30.9]

Fig. 7-30 Error range comparison with Liu (unit: nm)

7.6.5　Comparing with Simple Hysteresis linearization Compensation

C. J. Wu et al. [35] proposed that using simple measurement-based hysteresis observer, with voltage feedback to linearize the hysteresis phenomenon followed with a by the tracking controller, while in this thesis, this compensation method control result is best. Four different reference signals (Stair signal, sine waves with frequencies under

84

`

30Hz, 60Hz, 100Hz of which the amplitude is 1.2 micro-meter respectively) are chosen to compare the tracking performance of these two methods.

It can be seen that the performance is almost equal at low frequency, and slightly improved in very high frequency(100hz), but the results of 30hz and 60hz are not as good as Wu's. The reason of this is the synchronized control algorithm increased the complexity which leads to a decrease in performance.

However, without synchronized control unit, the stage will drift heavily as shown in section 7.2. Wu's method can only promise the control effect of measurement point in center while with synchronization and customized linearization, the whole stage's movement is guaranteed.
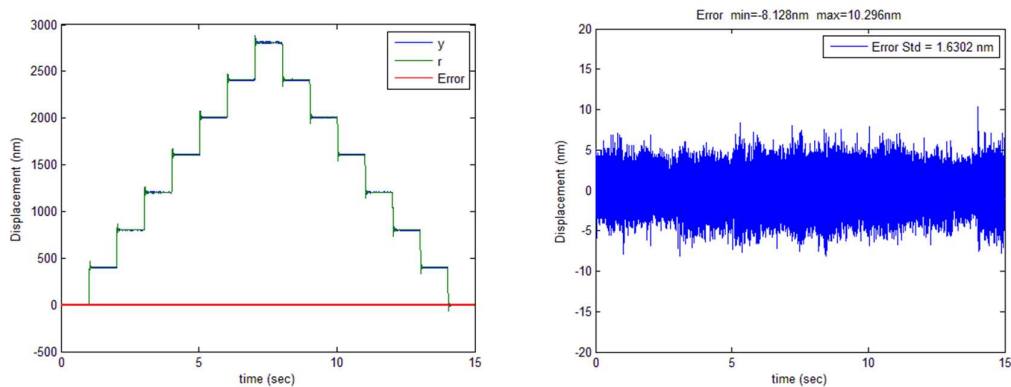
Fig. 7-31 Control result of stair signal from Wu
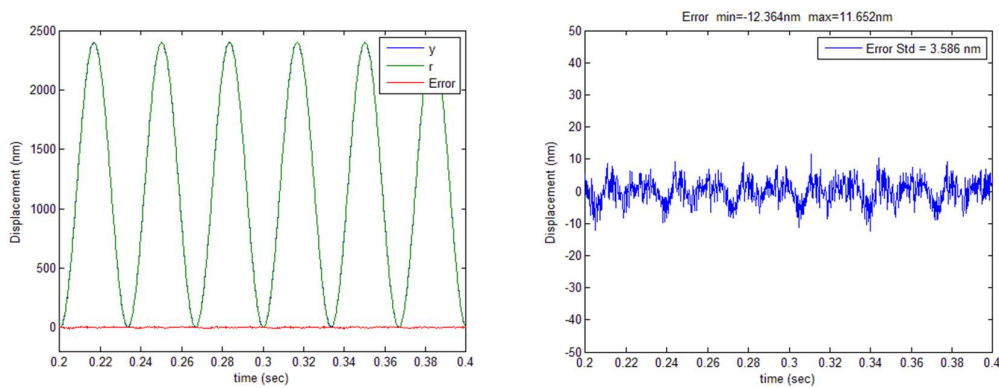

Fig. 7-32 Control result of 30Hz sine wave from Wu
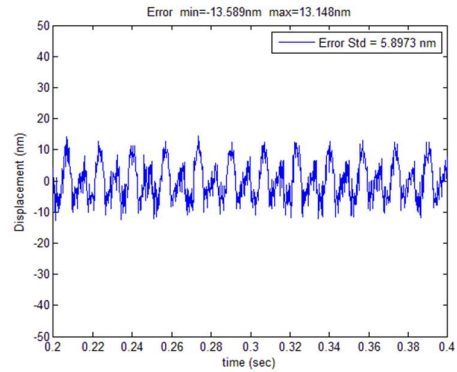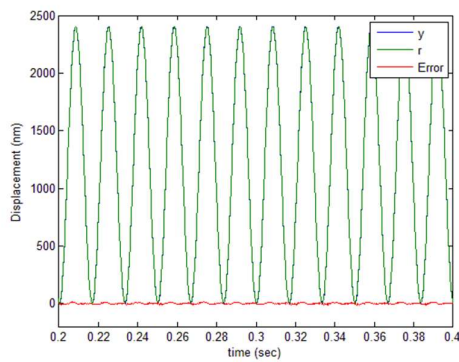
Fig. 7-33 Control result of 60Hz sine wave from Wu
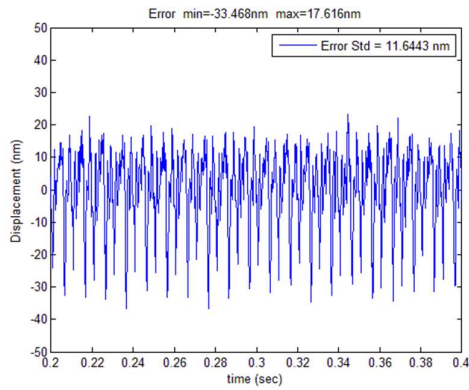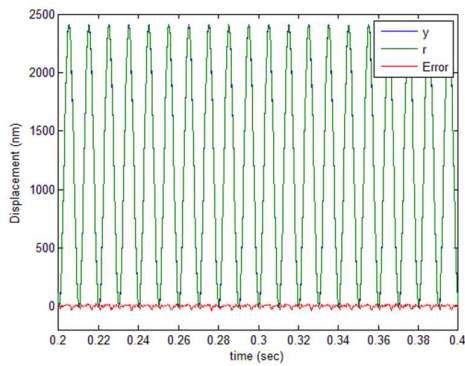
Fig. 7-34 Control result of 100Hz sine wave from Wu

	Stair	30Hz	60Hz	100Hz
Simple Lnearization	1.63	3.586	5.891	11.65
Synchronization & Linearization	3.0	5	7.1	11.2

Fig. 7-35 Standard deviation of the tracking error comparison with Simple

Linearization. (unit: nm)

	Stair	30Hz	60Hz	100Hz
Simple Linearization	[-8.2 , 10.3]	[-12.4 ,11.7]	[-13.5, 13.15]	[-33.5 , 17.6]
Synchronization & Linearization	[-12.4 , 11.2]	[-20.1 ,16.1]	[-19.7, 21.1]	[-36.3 , 30.9]

86

Fig. 7-36 Error range comparison with Simple Linearization (unit: nm)
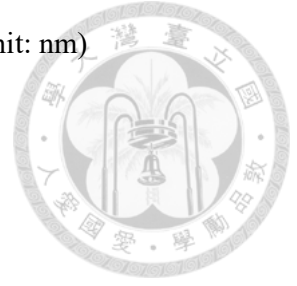
Chapter 8　Conclusions and Future Work
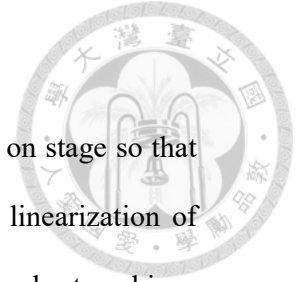
In this thesis, a cross-coupled synchronized control unit is applied on stage so that the consistency of two axes piezo actuators is guaranteed. Besides, a linearization of hysteresis phenomenon is utilized specially for every piezo-actuator in order to achieve precision positioning control. A modified Preisach model is used to simulate the hysteresis difference and compensate the nonlinearity caused by the hysteresis. The hysteresis differences of signals under different frequencies can be closely approximated by amplifying the differences of a static hysteresis model with certain gain. The movement difference of dual axes is compensated as well under all frequencies. With all of those techniques, the performance of the tracking signal is enhanced.

What's more, to improve the accuracy of tracking control, a PI controller and a feedback filter with a corner frequency are added as outer control loop.

Although now the synchronized unit is added under the cost of lower the overall performance, the balance taken after specific design. As tried before, too powerful synchronized unit is will result a huge influence on overall control that may cause unstable. On the other side, the performance of synchronization cannot meet requirement. However, the stability of dual axes pushing force should have improved the performance, this means there is still a space for reducing algorithm complexity and decoupling the system synchronization.

There's no doubt that the hysteresis linearization can effectually improve the performance of the tracking control,　but the relationship between the multiplied gain and the frequency of the input signal is still not formulated which still need to be decided mainly by experiments.

To proceed with this topic for practical and industrial usage, the author suggests

`

following points for further research:
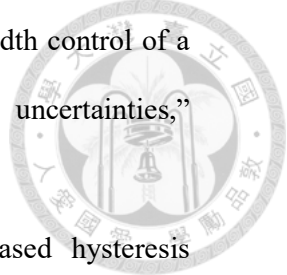
1. Observe and formulate the relationship between the differences of hysteresis phenomena while the frequency of the signal changes.

2. Self-tuning linearization and synchronization design to set parameters automatically so that the process of duplicated experiments can be omitted

3. Decoupling the system in a more proper way so that it not only reducing overall complexity but also makes the overall performance better than individual overall performance without synchronization.
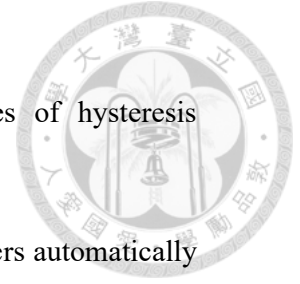
REFERENCE

[1] G. Song, J. Zhao, and J. De Abreu-Garcia, "Tracking control of a piezoceramic actuator with hysteresis compensation using inverse Preisach model," *IEEE/ASME Trans. Mechatronics*, vol. 10, no. 2, pp.198-209, Apr. 2005.

[2] S. Mittal and C-H. Menq, "Hysteresis compensation in electromagnetic actuators through Preisach model inversion," *IEEE/ASME Trans. Mechatron.*, vol. 5, no. 4, pp. 394–409, 2000.

[3] Y. Qin, Y. Tian, D. Zhang, B. Shirinzadeh and S. Fatikow "A novel direct inverse modeling approach for hysteresis compensation of piezoelectric actuator in feedforward applications," *IEEE/ASME Trans. Mechatronics*, vol. 18, no. 3, pp.981-989, 2013.

[4] F. Preisach, "Über die magnetische nachwirkung," Zeitschrift für Physik, vol. 94, pp. 277-302, 1935.

[5] I. D. Mayergoyz, *Mathermatical Models from the mathematical and control theory points of view*, J. Appl. Phys. vol. 57, pp. 3803-3805, 1985.

[6] I. D. Mayergoyz, *Mathermatical Models of Hysteresis*, 1990 :Springer-Verlag.

[7] I. D. Mayergoyz, "Dynamic preisach models of hysteresis," *IEEE Trans. Magn.*, vol. 24, no. 6, pp.2925 -2927, 1988.

[8] Y. Bernard, E. Mendes, and F. Bouillault, "Dynamic hysteresis modeling based on Preisach model," *IEEE Trans. Magn.*, vol. 38, pp. 885–888, 2002.

[9] S. Xiao and Y. Li, "Modeling and high dynamic compensating the rate-dependent hysteresis of piezoelectric actuators via a novel modified inverse preisach model," *IEEE Trans. Control Syst. Technol.*, 2013.

[10] S. S. Aphale, S. Devasia, and S. O. R. Moheimani, "High-bandwidth control of a piezoelectric nanopositioning stage in the present of plant uncertainties," *Nanotechnology*, vol. 19, pp. 125503-1–125503-9, 2008.

[11] J. A. Yi, S. Chang and Y. T. Shen "Disturbance-observer-based hysteresis compensation for piezoelectric actuators," *IEEE/ASME Trans. Mechatronics*, vol. 14, no. 4, pp.456 -464, 2009.

[12] C. J. Kemf and S. Kobayashi, "Disturbance observer and feedforward design for a high-speed direct-drive positioning table," *IEEE Trans. Contr. Syst. Technol.*, vol. 7, pp.513-526, 1999.

[13] S. M. Shahruz, "Performance enhancement of a class of nonlinear systems by disturbance observers," *IEEE/ASME Trans. Mechatronics*, vol.5, no.3, pp. 319–323, Sep. 2000.

[14] H. Shim and N. Jo, "An almost necessary and sufficient condition for robust stability of closed-loop systems with disturbance observer," *Automatica*, vol. 45, pp. 296–299, 2009.

[15] H. J. M. Adriaens, W. L. de Koning and R. Banning "Modeling piezoelectric actuators," *IEEE/ASME Trans. Mechatronics*, vol. 5, no. 4, pp.331 -341, 2000.

[16] L. S. Chen, J. Y. Yen, *et al.*, "Precision Tracking of a Piezo-Driven Stage by Charge Feedback Control," *Precision Engineering*, 2013.

[17] R.D.Lorenz, P.B.Schmidt, "Synchronized motion control for process automation,",*Proceedings of the 1989 IEEE Industry Applications Annual Meeting*,pp.1693-1698,1989

[18] Y,Koren, "Cross-coupled biaxial computer control for manufacturing systems", *Journal of Dynamic System, Measurement, and Control*,Vol.102,pp.265-272,1980

[19] Wen-Bin Shih, "Adaptive Fuzzy Controller Design for Permanent Magnet

Synchronous Motor Systems," Master thesis, Department of Electrical Engineering, Yuan Ze University, 2007.
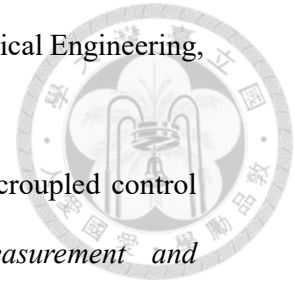
[20] S.S.Yen, P.L.Hsu, "Theory and applications of the robust crpss-croupled control design," *ASME Trans. Journal of Dynamic Systems, Measurement and Control*,Vol.121,pp.524-530,1999

[21] Physik Instrumente Inc., *The world of micro- and nanopositioning*, 2005/2006.

[22] Physik Instrumente GmbH, Tutorial: Piezoelectrics in Nanopositioning, Designing with Piezoelectric Actuators, 2009.

[23] Piezomechanik, *Low voltage co-fired multilayer stacks, rings and chips for actuation*, pp. 21-23, 2004.

[24] Q. Yao, Jingyan Dong and Placid M. Ferreira, "A novel parallel-kinematics mechanisms for integrated, multi-axis nanopositioning: Part 2. Dynamics, control and performance analysis," *Precision Engineering*, Vol. 32, Issue 1, pp.20-23, Jan. 2008.

[25] Y. Tian, B. Shirinzadeh, and D. Zhang. "Design and dynamics of a 3-DOF flexure-based parallel mechanism for micro/nano manipulation," *Microelectronic Engineering*, Vol. 87, pp. 230-241, 2010.

[26] Agilent Technologies Inc., "Chapter 7B Agilent 10705A Single Beam Interferometer," in *Laser and Optics User's Manual*, 2002.

[27] A. Visintin, "Mathematical models of hysteresis," in *The Science of Hysteresis*, G. Bertotti and I. Mayergoyz, Eds. London, U.K.: Academic, 2006, pp. 1–123.

[28] C. Y. Su, Y. Stepanenko, J. Svoboda, and T. Leung, "Robust adaptive control of a class of nonlinear systems with unknown backlash-like hysteresis," *IEEE Trans. Autom*. Control,vol.45,no.12,pp.2427–2432, Dec. 2000.

[29] L. Ljung, *System Identification Toolbox—User's Guide*, Mathworks, Sherborn, MA,

2003.

[30] T. Katayama, *Subspace Methods for System Identification*, Springer, 2005.

[31] M. Tomizuka, "Zero phase error tracking algorithm for digital control," *Journal of dynamic systems, measurement, and control*, Vol. 109, pp 65-68, 1987.

[32] E. Gross, M. Tomizuka, and W. Messner. "Cancellation of discrete time unstable zeros by feedforward control." *Journal of dynamic systems, measurement, and control*, Vol. 116, pp. 33-38, 1994.

[33] J. A. Butterworth, L. Y. Pao and D. Y. Abramovitch, "The effect of nonminimum-phase zero locations on the performance of feedforward model-inverse control techniques in discrete-time systems," *American Control Conference*, 2008.

[34] H. F Tsai, "Hysteresis compensation of piezoelectric-actuated stage by surface fitted inverse Preisach model and robust control," Master thesis, Department of Mechanical Engineering, National Taiwan University, 2012.

[35] C. Z. Jan, "Piezo-Stage Identification and Control Based on Non-Hysteretic Electromechanical with Charge input," Master thesis, Department of Mechanical Engineering, National Taiwan University, 2013.

[36] S. F. Wen, "Charge Feedback Hysteresis Disturbance Observer Design of a Multi-axis Piezo-actuated Stage," Master thesis, Department of Mechanical Engineering, National Taiwan University, 2014.

[37] L. S. Chen, "Sensorless Precision Motion Control of a Multi-axis Piezo-actuated Stage," Ph.D. dissertation, Department of Mechanical Engineering, National Taiwan University, 2013.

[38] F. C. Wang, L. S. Chen, Y. C. Tsai, C. H. Hsieh and J. Y. Yen, "Robust loop-shaping control for a nano-positioning stage," *Journal of Vibration and Control*, 2013.

[39] S. T. Liu, "A Hybrid Hysteresis Compensation of Hysteresis Observer and Preisach

Model Estimator for Pizeo-actuated Stage," Master thesis, Department of Mechanical Engineering, National Taiwan University, 2015.

[40] C.J. Wu, "Frequency effect on the hysteresis phenomenon and its control strategy," Master thesis, Department of Mechanical Engineering, National Taiwan University, 2016.

[41] R.Y. Chiang, *Robust Control Toolbox Toolbox—User's Guide,* Mathworks, Sherborn, MA, 2003.